The EMC Effect in Spin Structure Functions

A 12 GeV Proposal to Jefferson Lab PAC 42

May 22, 2014

W. K. Brooks[1], H. Hakobyan, B. Kopeliovich, S. Kuleshov, S. Mancilla, and R. Mendez
Universidad Técnica Federico Santa María, Valparaíso, Chile

K. Adhikari, G. Dodge, L. El Fassi, S. Kuhn[2], and L. Weinstein
Old Dominion University, Norfolk, VA 23529

H. Avakian, A. Deur, D. Higinbotham, C. Keith, W. Melnitchouk and J. Pierce
Thomas Jefferson National Accelerator Facility, Newport News, VA 23606

D. Crabb, D. Keller, S. Tkachenko, and J. Zhang
University of Virginia, Charlottesville, VA 22901

P. E. Bosted and K. Griffioen
The College of William and Mary, Williamsburg, VA 23187
and *Thomas Jefferson National Accelerator Facility, Newport News, VA 23606*

K. Hicks
Ohio University, Athens, OH 45701

R. Dupré
Université Paris-Sud, Institut de Physique Nuclaire d'Orsay, Orsay, France

T. Badman, S. Li, E. Long, K. Slifer, P. Solvignon, R. Zielinski
University of New Hampshire, Durham, NH 03824

N. Kalantarians
Hampton University, Hampton, VA 23668

F.J. Klein
Catholic University, Washington, DC 20064

A. W. Thomas
The University of Adelaide, Adelaide SA 5005, Australia

W. Bentz
Tokai University, 1117 Kitakaname, Hiratsuka-shi, Kanagawa 259-1292, Japan

I. Cloet, R.B. Wiringa
Argonne National Laboratory, Argonne, Il 60439

C. Ciofi degli Atti
INFN Sezione di Perugia, I-06100 Perugia, Italy

H. Fanchiotti, C.A. García Canal, T. Tarutina
Dept. de Física and IFLP (CONICET), Univ. Nacional de La Plata, C.C. 67-1900 La Plata, Argentina

V. Vento
Dept. de Física Teórica and Instituto de Física Corpuscular, Univ. de Valencia, 46100 Burjassot (Valéncia), Spain

and the CEBAF Large Acceptance Spectrometer **collaboration**

Abstract

We propose to perform the first measurements of the spin-dependent EMC effect utilizing CLAS12 in Hall B with 11 GeV polarized electrons and polarized nuclear targets. Our target of choice is ^{7}Li (in the form of dynamically polarized ^{7}LiD) in which a highly polarized proton is embedded in the nuclear medium. Simultaneously, we will also measure the double spin asymmetry on the proton with a ^{6}LiH target, to minimize systematic uncertainties. The experiment will obtain the double spin asymmetry $A_{||}^{^7Li} \approx g_1^{^7Li}/F_1^{^7Li}$ from the measurement on ^{7}LiD, after correcting for the small contribution from other polarized species (D) and the beam and target polarization as well as the dilution by unpolarized target components. Using the simultaneous measurement on ^{6}LiH, we can form the ratio of the double spin asymmetries as well as the cross section differences directly (with many systematic uncertainties canceling), both of which contain direct information on any medium effect on spin structure functions and asymmetries. Together with the unpolarized structure function (to be measured in Hall C), we can also extract $g_1^{^7Li}$ and, using a sophisticated modern wave function model, finally the "in-medium" spin structure function function $g_1^{p|^7Li}$ for a proton bound in ^{7}LiD. We will cover a kinematic range of $1 < Q^2 < 15$ GeV^2 and $0.06 < x < 0.8$. These data will provide new constraints on models for the EMC effect, some of which predict that medium modifications of quark distributions depend strongly on the quark helicities.

We request 50 days of 11 GeV beam on the longitudinal polarized target and 5 additional days for auxiliary measurements.

CONTENTS

I. PHYSICS

A. Introduction

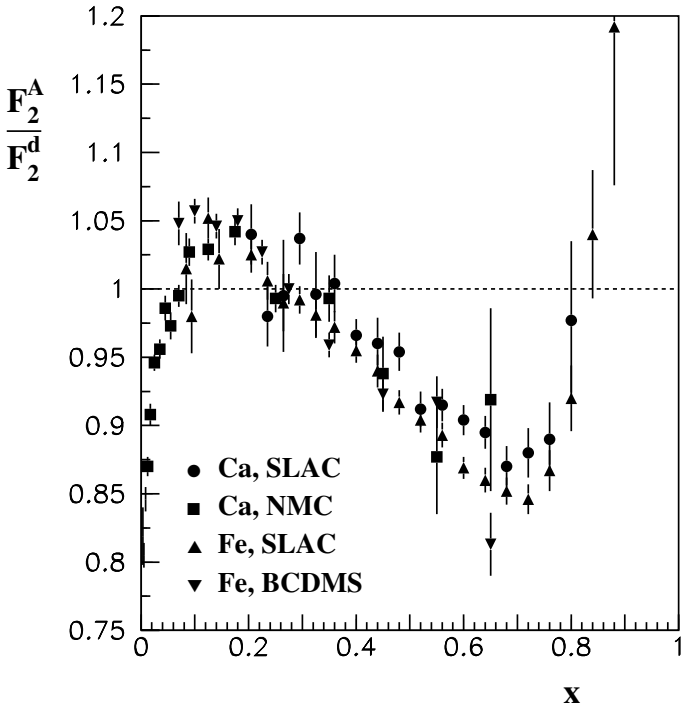

FIG. 1. Experimental data for the EMC effect in the unpolarized structure function F_2 for ^{40}Ca and ^{56}Fe taken at NMC, SLAC and BCDMS.

The question of how the properties of nucleons bound in the nuclear medium differ from the properties of free nucleons is a fundamental problem at the intersection of particle and nuclear physics. We cannot truly claim to understand hadron structure, the strong interaction, and the binding of nucleons in nuclei until we have a rigorous, QCD-based understanding of this problem. However, more than 30 years after the European Muon Collaboration (EMC) at CERN first published their results on the modification of nucleon structure functions in the nucleus [3], there is still no complete and universally agreed-upon explanation of this "EMC effect".

Some of the early data on the ratio of nuclear to nucleon inclusive structure functions, from SLAC [4, 5], NMC [6] and BCDMS [7], are shown in Fig. 1. One can roughly distinguish 4 kinematic regions: A suppression of the nuclear structure functions at very low x (known as "shadowing" and reasonably well understood as a consequence of coherent scattering on more than one nucleon), an enhancement between $x = 0.1$ and $x = 0.2$, and a downward slope at larger x which eventually turns back up (above $x \approx 0.7$) due to the effect of nucleon Fermi motion inside the nucleus. These features are quite universal for all nuclei, but the amplitude (maximum deviation from unity) depends strongly on the nucleus under study. In particular the higher x region (often considered the "EMC effect proper") is still a source of controversy. Here, the downward slope of the ratio of structure functions seems to indicate a modification of the valence quark structure of the nucleon. While the consensus is pretty clear that nuclear binding effects alone cannot explain the full depletion around $x = 0.6 - 0.7$, at least two different fundamental mechanisms have been proposed to explain such a modification (see also next Section):

- One possibility is that it is a "mean field in medium effect", where nucleons inside the nuclear medium experience an average distortion or a change in their internal quark distribution functions due to a "background field" that affects the quark momentum distribution [8]. In the same category fall explanations that model the EMC effect through "nucleon swelling" [9] or rescaling of the Bjorken variable x [10] due to the binding of nucleons in nuclei.

- Alternatively, it has been argued that the modification is directly proportional to the "off-shell-ness" of the struck nucleon, which is related to its initial momentum. In this picture, the EMC effect is an averaging between nearly

unmodified, slow-moving "mean field" nucleons and strongly modified, far off-shell high-momentum nucleons that are part of a short-range correlation pair (see, *e.g.*, [11, 12] and references therein).

In addition, there are models of the EMC effect invoking non-nucleonic degrees of freedom (pions, Deltas, multi-quark clusters [13]).

More precise measurements of the unpolarized EMC ratio, while necessary (and already approved for the 12 GeV program at Jefferson Lab [14, 15]), may not be able to distinguish between these two possibilities, since nuclei with higher "local density" [16] tend to have *both* a higher probability of high-momentum components in the nuclear wave function *and* deeper average binding, (*i.e.*, a stronger mean field). More direct methods, like tagging high momentum struck nucleons by high momentum spectators [17, 18] can give more specific information, but their interpretation is difficult because of final state interactions and other possible violations of the spectator picture. In this context, the spin-dependent EMC ratio has the potential to add new and complementary information, especially in cases like ^{7}Li where (according to all modern nuclear models) nearly all of the nuclear spin is carried by a single proton. Therefore, one can probe more directly the modification of that *one* nucleon as opposed to an average over all nucleons in the nucleus. There are several predictions for this new polarized EMC effect, which differ significantly in both the strength and the x-dependence they predict. On the other hand, nothing is known experimentally at this point.

The proposed measurement will therefore establish a first benchmark and may very well yield surprises commensurate with the original EMC effect. We believe such a measurement is the missing corner stone in the multi-pronged attempt to finally settle the question of the origin of the EMC effect with Jefferson Lab at 12 GeV. At the same time, there are several high-precision experiments approved for the 12 GeV program that aim to extract information on neutron spin structure functions from measurements on ^{3}He and the deuteron. We believe that the proposed measurement will help us decide which models of the polarized EMC effect should be used to correct these data for nuclear effects, which may turn out to be essential to keep these model uncertainties below the level where they may impact the ultimate precision of these experiments.

B. Background

The modification of hadron properties in the nuclear environment is of fundamental importance in understanding the implications of QCD for nuclear physics. Understanding the origin of such medium effects in a microscopic way is a crucial building block for a complete picture of confinement and nuclear binding in QCD. Equally important, for the extraction of "free" nucleon spin structure functions from nuclei (in particular the deuteron and ^{3}He), a better understanding of their possible modifications in medium is crucial to realize the full potential of high-precision measurements planned both at Jefferson Lab at 12 GeV and for the future EIC.

Since the original publication of the "EMC effect", a truly staggering number of publications have appeared that attempt to describe various (or all) of the features observed in the data. (For a summary, see for instance [19] and, more recently, [12, 20, 21] and references therein). In particular, several approaches have been used to explain the observed nuclear dependence in the region $0.2 < x < 0.7$. Some models have attempted to describe the EMC effect in this region using conventional nuclear physics employing nucleonic and pionic degrees of freedom [22–24]. Another category of models has assumed the existence of exotic states such as multiquark clusters in nuclei [13]. A different approach used by rescaling models postulates that the scale Q^2 [9] or the variable x [10] for a bound nucleon is different from that of a free nucleon. There are recent calculations based on modifications of quark distribution in the nuclear mean field [25]. In contrast, several recent publications emphasize the connection between the EMC effect and the high-momentum components of the nuclear wave function due to short-range correlations [12, 20].

On the experimental side, a large number of high precision experiments have recently been completed at Jefferson Lab. In particular, data on few-body nuclei reveal [16] that the strength of the EMC effect is not a simple function of the nuclear baryon number, A, or the assumed average nuclear density, $A/(4\pi R^3/3)$, where R is the average nuclear radius. Instead, in particular data on ^{9}Be seem to support a picture where this strength is related to the *local* nuclear density as seen by the struck nucleon. Further corroboration of this picture comes from the observation that the strength of the EMC effect (the magnitude of the slope between $x = 0.3$ and $x = 0.7$) is tightly correlated with the probability to find a two-nucleon short-range correlation inside the nucleus, as indicated by the relative strength of the quasi-elastic response in the $x > 1.3$ region [12]. It is reasonable to assume that such short-range correlations are more probable in nuclei where nucleons are on average closer to each other (larger local density). However, it is not *a priori* clear whether it is those high-momentum nucleons that contribute predominantly to the EMC effect, or whether it is an average medium effect that is enhanced in regions of larger local density.

Surprisingly, polarization degrees of freedom have been largely ignored, in particular experimentally. Quite a few theoretical predictions exist [13, 25–30], which we will discuss in more detail in Section I D. However, there are no experimental data at all (with the possible exception of the b_1 structure function of the deuteron, measured first by the

HERMES collaboration [31] and proposed for measurement at JLab with 12 GeV [32]). The relatively smaller number of theoretical predictions until fairly recently is most likely due to the absence of data; in fact, since the measurement discussed here was first proposed to the Jefferson Lab PAC [33], several new publications have appeared [29, 30]. A significant number of theorists have signed on to the present proposal, showing that such data are eagerly awaited.

The development of a decisive measurement of the polarized EMC effect, as proposed here, has been hampered by several (perceived or real) difficulties (see also previous PAC and TAC reports on the 6 GeV [33] and 12 GeV [34] letter-of-intent versions of this proposal):

1. There is an absolute conservation of baryon number in QCD, which guarantees that any modification of the nucleon structure cannot change the total number of valence quarks. This seems to favor a clear and unambiguous definition of what we mean by "modification of the nucleon structure". In contrast, spin is *not* a conserved quantity (only total angular momentum is), so a priori a modification of the "bound nucleon spin structure function" seems less clearly distinct from well-known "standard nuclear effects", i.e., spin-orbit coupling for individual nucleons and spin-spin coupling between different nucleons.

2. Within most nuclear models (and for most nuclei), typically only one or two nucleons carry significant spin polarization, even in a 100% polarized nucleus. This means that any spin-dependent effects are "diluted" by factors of order $1/A$ or $2/A$. This is in contrast with the spin-averaged EMC effect, which in principle affects all nucleons equally (depending on one's model).

3. Experimentally, nuclear targets are often more difficult to polarize to a high degree, and the necessary techniques and knowledge are less broadly available than that for polarized hydrogen, deuterium and Helium-3 targets which have been used in numerous spin structure function experiments.

In this proposal, we will demonstrate that none of these issues prevents a statistically powerful and meaningful measurement that can directly test models of nucleon modifications including polarization degrees of freedom. Some of the details follow in later sections, but we would like to summarize some salient points in response to the three concerns above:

1. The difference between polarized and unpolarized EMC effect with respect to interpretability is not as large as this argument assumes. In both cases, one can define a "naïve" EMC ratio (Eqs. 24,23 below). These ratios have the advantage of being clearly defined experimentally, without reference to any nuclear model. However, even within standard nuclear physics (absent any nucleon modifications in the nucleus), neither one of these ratios would be reasonably expected to be equal to 1 - standard nuclear effects like Fermi motion and binding will modify both significantly. The fact that typically less than 100% of the nuclear angular momentum is carried by a single nucleon spin is just one more of these standard nuclear effects.

   Several attempts have been made to correct the unpolarized EMC ratio (Eq. 24) for at least some "obvious" nuclear effects - e.g. for the momentum fraction carried by equivalent photons in the IMF, and by redefining the scaling variable x to account for the overall reduction in nuclear mass due to binding [20]. Similar corrections (e.g., for the "effective nucleon polarizations" inside nuclei) have been applied in the polarized case (especially when attempting to extract "free" nucleon spin structure functions from measurements on the deuteron and Helium-3). Ultimately, in both cases, one should define a "EMC effect proper" as the ratio between the measured nuclear structure function and the best possible predictions of modern, realistic nuclear models containing only nucleon (and perhaps meson) degrees of freedom. Such sophisticated nuclear models are becoming increasingly available and can be used for both polarized and unpolarized data, in particular for few-body nuclei ($A < 12-16$).

   Our main approach will be to extract the "naïve" EMC ratios from our data and compare them with both state of the art standard nuclear models as well as models (to be described below) that contain an explicit change in the internal nucleon structure. Of course, our data will be available to compare to future, further improved calculations without any prejudice or model-dependence built in.

2. Apart from the question "how much of the nuclear spin is carried by the valence nucleon(s) in the nucleus", one also has to contend with the dilution of the signal from this nucleon (or these nucleons) by the typically unpolarized (or only slightly polarized) nucleons making up the bulk of the nucleus. For example, in ^{7}Li, all modern calculations show that about 86% of the nuclear spin is carried by a single valence proton, while two $1p3/2$ neutrons (in shell model notation) are only slightly polarized and the doubly magic "^{4}He core" has net polarization of zero for all its four nucleons. Since this situation becomes increasingly less favorable for heavier nuclei, we believe that ^{7}Li is a good compromise - the nucleus is dense enough to expect a sizable EMC effect (both polarized and unpolarized) but the "dilution" of $\approx 1/7$ of the polarized EMC effect is not yet unreasonably large (in fact, as shown later, the dilution is actually more favorable, due to the larger proton

cross section). In any case, we demonstrate that we will have sufficient statistical precision to measure the somewhat reduced double spin asymmetry $A_{||}$ (see Eq. 6) on ^{7}Li to a meaningful level when compared to the corresponding asymmetry on the proton. Since the extracted "naïve" EMC ratio is nearly directly proportional to the ratios of these asymmetries (assuming data on the unpolarized structure functions from other approved experiments [14]), only the relative uncertainty on both is relevant.

Beyond this, we would like to argue that, apart from a technical difficulty, this "dilution" is actually a virtue of polarized experiments. This is because progress in our understanding of the EMC effect requires new evidence whether it uniformly affects all nucleons, or rather is a consequence of rare quantum fluctuations (due to SRC etc.). Having the polarized EMC ratio determined, to a large extent, by a single nucleon with *known* wave function inside the nucleus can provide a decisive step in this direction. For example, in certain models of the EMC effect [35] it is assumed that the medium modification of nucleon structure is much stronger for the most deeply bound nucleons than for those with the smallest removal energy. If this is true, one would expect a *smaller* EMC effect for polarized structure functions, since it is universally true that the least-bound nucleons tend to be the ones that carry (most of) the spin quantum numbers of their host nucleus. On the other hand, at very low x, the effects from shadowing are actually *enhanced* by a factor of about 2 if one deals with a single nucleon that carries the quantity measured [28].

3. We believe that the technical difficulties for polarizing ^{7}Li to a high degree are reasonably well understood. We are proposing a target design that minimizes systematic errors due to any imprecision in the determination of nuclear or nucleon polarizations. We also propose several cross checks to test both our understanding of the target and standard nuclear models of ^{7}Li. Finally, we point out that a good fraction of the active world experts in polarized target technology have signed on to this proposal, providing us with confidence that we can carry out any necessary development and prototyping work.

C. Notation

For a free nucleon (and any spin-1/2 hadron), there are two independent structure functions in the Bjorken limit ($Q^2 \to \infty, x$ fixed) that describe the (helicity-dependent) inclusive electron scattering cross section: F_1 and g_1 [36]. At finite momentum transfer, Q^2, there are additional structure functions that encode deviations from the simple Callan-Gross relationship and leading twist. For the following, we choose to express these higher–order terms through the ratio $R = \sigma_L/\sigma_T$ for longitudinal over transverse virtual photon absorption cross sections, and the virtual photon transverse-longitudinal interference asymmetry A_2. A_2 is constrained by the Soffer inequality [37, 38]:

$$|A_2| \leq \sqrt{R\,(1+A_1)/2}. \tag{1}$$

For completeness, we also express other often–used structure functions (including the transverse virtual photon absorption asymmetry A_1) in terms of this set:

$$\begin{aligned}
F_2(x,Q^2) &= 2xF_1(x,Q^2)\frac{1+R(x,Q^2)}{1+\gamma^2} \to 2xF_1(x) \\
g_T(x,Q^2) &= F_1(x,Q^2)\frac{A_2(x,Q^2)}{\gamma} \to \int_x^1 g_1(y)\frac{dy}{y} \\
g_2(x,Q^2) &= g_T(x,Q^2) - g_1(x,Q^2) \\
A_1(x,Q^2) &= \frac{g_1(x,Q^2)-\gamma^2 g_2(x,Q^2)}{F_1(x,Q^2)} = (1+\gamma^2)\frac{g_1(x,Q^2)}{F_1(x,Q^2)} - \gamma A_2(x,Q^2) \to \frac{g_1(x)}{F_1(x)},
\end{aligned} \tag{2}$$

with the usual Bjorken variable $x = Q^2/2M\nu$ and $\gamma = \sqrt{Q^2}/\nu$, where M is the nucleon mass and ν the energy transferred to the nucleon in its rest frame. All structure functions defined are functions of both Q^2 and x or the final state mass $W = \sqrt{M^2 + 2M\nu - Q^2}$. The right-most expressions in Eq. 2 show the asymptotic behavior in the Bjorken limit and at leading twist. The expression for g_T is the Wandzura-Wilczek relation [39].

For an electron beam with helicity $+(-)$ scattering off a nucleon with its spin oriented opposite to the electron beam direction, one can write the cross section as

$$\frac{d\sigma^{+(-)}}{d\Omega dE'} = \sigma_M \left[\frac{F_2}{\nu}\frac{1+\epsilon R}{\epsilon(1+R)} \pm 2\tan^2\frac{\theta_e}{2}\left(\frac{E+E'\cos\theta_e + Q^2/\nu}{M\nu} g_1 - \frac{2xF_1A_2}{\sqrt{Q^2}}\right)\right], \tag{3}$$

where the Mott cross section

$$\sigma_M = \frac{4E'^2\alpha^2\cos^2\frac{\theta}{2}}{Q^4} \tag{4}$$

and the virtual photon polarization ratio

$$\epsilon = \left(1 + 2[1+1/\gamma^2]\tan^2\frac{\theta_e}{2}\right)^{-1}, \tag{5}$$

all in terms of the the initial (E) and final (E') electron energy in the nucleon rest system, and the electron scattering angle θ_e.

For the following, it is also useful to write down the double spin asymmetry

$$A_{||} = \frac{d\sigma^+ - d\sigma^-}{d\sigma^+ + d\sigma^-} = D\left(A_1(\nu,Q^2) + \eta A_2(\nu,Q^2)\right) = D\left((1+\gamma^2)\frac{g_1}{F_1} + (\eta-\gamma)A_2\right). \tag{6}$$

Here,

$$D = \frac{1-\epsilon E'/E}{1+\epsilon R}, \tag{7}$$

and

$$\eta = \frac{\epsilon\sqrt{Q^2}}{E-\epsilon E'}. \tag{8}$$

For a nuclear target ($A > 1$), one can in principle write down the same equations. However, one may have to distinguish among the $(2J+1)$ possible spin projections of the target, if the latter has spin $J > 1/2$. So, in principle, one has to define structure functions like F_{2A}^{JM} and g_{1A}^{JM} for each projection M of the nuclear spin along the z-axis [25] (in our case, opposite to the beam direction). Symmetry considerations (like parity conservation in the strong and electromagnetic interactions) show that one only has to consider states with $M_J > 0$, since the following relationships hold:

$$F_{2A}^{J\ -M} = F_{2A}^{J\ M}; g_{1A}^{J\ -M} = -g_{1A}^{J\ M}. \tag{9}$$

This also explains why for the nucleon, with Spin 1/2, only one version for F_2 and g_1 each have to be considered.

For a target with Spin 1 (e.g., the deuteron), we have one beam spin-dependent structure function, $g_{1D}^{1\ +1}$ and *two* beam-helicity **in**dependent structure functions, $F_{2D}^{1\ +1}$ and $F_{2D}^{1\ 0}$. Cloët, Bentz and Thomas [25] introduce a set of "multipole structure functions" that are linear combinations of the ones for each M; they behave properly under rotation (like the components of spherical tensors). For practical purposes, it is more straightforward to multiply these multipole structure functions with appropriate factors to allow us to express cross sections and cross section differences directly in terms of cartesian target polarization observables. In the case of Spin-1, there are two such observables: the vector polarization $P_z = n_+ - n_-$ and the tensor polarization $P_{zz} = n_+ + n_- - 2n_0$. Here, the n_M are the relative probabilities of each of the three possible spin projections M, normalized to add up to 1.

If we define

$$F_{2D}^0 = \frac{2}{3}F_{2D}^{1\ +1} + \frac{1}{3}F_{2D}^{1\ 0} \tag{10}$$

and

$$F_{2D}^{zz} = \frac{2}{3}\left(F_{2D}^{1\ +1} - F_{2D}^{1\ 0}\right) \tag{11}$$

then the average cross section can be written

$$\frac{d\sigma^+ + d\sigma^-}{2} \propto F_{2D}^0 + \frac{1}{2}P_{zz}F_{2D}^{zz}. \tag{12}$$

Here, the proportionality factor is the equivalent of that multiplying F_2 in Eq. 3.

In the case of Spin-3/2 (e.g., ^{7}Li which is our proposed nucleus), there are three numbers that characterize the polarization state of the target (assuming symmetry around the z-axis), namely vector polarization:

$$P_z = n_{+3/2} + \frac{n_{+1/2}}{3} - \frac{n_{-1/2}}{3} - n_{-3/2}, \tag{13}$$

2nd-rank tensor polarization:

$$P_{zz} = n_{+3/2} - n_{+1/2} - n_{-1/2} + n_{-3/2}, \tag{14}$$

and 3rd-rank tensor polarization:

$$P_{zzz} = \frac{n_{+3/2}}{3} - n_{+1/2} + n_{-1/2} - \frac{n_{-3/2}}{3}. \tag{15}$$

Now, both F_2 and g_1 occur twice. We can again define "practical" linear combinations, namely

$$F_{2A}^0 = \frac{1}{2}F_{2A}^{3/2\ +3/2} + \frac{1}{2}F_{2A}^{3/2\ +1/2} \tag{16}$$

and

$$F_{2A}^{zz} = F_{2A}^{3/2\ +3/2} - F_{2A}^{3/2\ +1/2} \tag{17}$$

with the same result for the average cross section as for Spin-1. Note that the definition of these structure functions was chosen such that in an extreme independent-nucleon picture of the nucleus (with all nucleons at rest and free), one would "automatically" have $F_{2A}^0 = ZF_{2p} + NF_{2n}$ with $A = Z + N$, and $F_{2A}^{zz} = 0$.

The polarized structure functions can be defined as

$$g_{1A}^z = \frac{9}{10}g_{1A}^{3/2\ +3/2} + \frac{3}{10}g_{1A}^{3/2\ +1/2} \tag{18}$$

and

$$g_{1A}^{zzz} = \frac{3}{10}g_{1A}^{3/2\ +3/2} - \frac{9}{10}g_{1A}^{3/2\ +1/2}. \tag{19}$$

This yields for the cross section half-difference

$$\frac{d\sigma^+ - d\sigma^-}{2} \propto P_z g_{1A}^z + P_{zzz} g_{1A}^{zzz} + P_z C(A_2) \tag{20}$$

again with the same proportionality factor as in Eq. 3. (Here, $C(A_2)$ is a correction analogous to the last term in Eq. 3, see below and Section II C. We note that A_2^p has been measured by several Jefferson Lab experiments, including RSS and SANE in Hall C.)

The definitions for the two spin-dependent structure functions have been chosen such that, for a nucleus where a single (free) nucleon carries all its quantum numbers (e.g., a single proton in the $1p_{3/2}$ shell of ^{7}Li), we get (ignoring nucleon motion)

$$g_{1A}^z = g_{1N} \tag{21}$$

and

$$g_{1A}^{zzz} = 0. \tag{22}$$

Hence, the "tensor structure functions" F_{2A}^{zz} and g_{1A}^{zzz} carry direct information on nuclear binding effects, including Fermi motion, and are expected to be small.

We can now define the *polarized EMC ratio* as

$$R_{pol} = g_{1A}^z / g_{1N}, \tag{23}$$

where "N" stands for p in the case of ^{7}Li and in general for the nucleon that carries the angular momentum quantum numbers of the nucleus in question (it would be the average of p and n in the case of nuclei like the deuteron and ^{6}Li where both nucleons contribute equally). The usual (unpolarized) EMC ratio is recovered as

$$R_{unpol} = \frac{F_{2A}^0}{ZF_{2p} + NF_{2n}}. \tag{24}$$

Finally, we note that the double spin asymmetry will be proportional to

$$A_{||\ ^7Li}^{meas} = \frac{N^+ - N^-}{N^+ + N^-} \propto P_z \frac{g_{1A}^z + \frac{P_{zzz}}{P_z} g_{1A}^{zzz} + C(A_2)}{F_{2A}^0 + \frac{1}{2} P_{zz} F_{2A}^{zz}}. \tag{25}$$

In principle, the denominator can be determined from the approved measurement of unpolarized structure functions of various nuclei [14], after applying a small correction for the contribution $\frac{1}{2} P_{zz} F_{2A}^{zz}$ which will not be present in that experiment. We expect P_{zz} to be about 0.5 (see Section II A), while the structure function F_{2A}^{zz} is expected to be at least an order of magnitude smaller than F_{2A}^0 and can be calculated precisely in standard nuclear models of ^{7}Li. Any "EMC type effect" modifying F_{2A}^{zz} would be a small correction on top of a correction; in any case, it could be viewed as part of the overall spin-dependent "EMC effect" we seek to measure. To extract the sought-after structure function $g_{1A}^z(x, Q^2)$, we would have to correct for the small contributions to the numerator from g_{1A}^{zzz} and the term involving A_2. Similar arguments apply here: Both terms can be precisely calculated within the "standard nuclear model" and subtracted. In addition, the tensor polarization P_{zzz} multiplying g_{1A}^{zzz} will be very small, of order 10% of P_z. And finally, once again any non-standard contributions to this term should be considered part of the "polarized EMC effect" in ^{7}Li.

However, combining two different experiments to extract the sought-after "polarized EMC ratio" (Eq. 23) could lead to additional systematic uncertainties; for this reason, we are proposing to measure two related (but slightly different) ratios that rely only on data collected within the experiment proposed here. These ratios can also be compared to state-of-the art "nucleons-only" nuclear model calculations and therefore serve as a direct test of the polarized EMC effect in ^{7}Li. The first of these is the ratio of the *cross section difference* for opposite target polarization for ^{7}Li and the proton. While it is in principle more difficult to measure cross sections (and their differences) directly (requiring good knowledge of both target density, integrated beam charge and detector acceptance and efficiency), many of the unknown quantities cancel in the experimental set up we propose (see Section II). From Eqs. (3,20), it follows that this ratio (which we assume has been normalized to the respective target polarizations P_z) can be expressed as

$$R_1 = \frac{[d\sigma^+ - d\sigma^-]_{^7\mathrm{Li}}}{[d\sigma^+ - d\sigma^-]_p} = \frac{g_{1^7\mathrm{Li}}^z + \frac{P_{zzz}}{P_z} g_{1^7\mathrm{Li}}^{zzz} + C_{^7\mathrm{Li}}(A_2)}{g_1^p + C_p(A_2)} \tag{26}$$

Given a suitable parametrization for g_1 and A_2, all terms in Eq. 26 can be calculated within a standard nuclear model.

The second ratio takes the asymmetry Eq. 25 and divides it by the corresponding asymmetry (Eq. 6) on the proton. By measuring both asymmetries simultaneously, several potentially uncertain factors drop out, and (as we will show below) model dependencies are minimized. Of course, even in an extreme "independent nucleons" model of ^{7}Li, this asymmetry ratio would not be equal to 1, since the denominator in one case is the ^{7}Li unpolarized structure function F_2, while in the other case, it is the proton one. For purely "optical" reasons, we therefore multiply this ratio (in our discussion in Section II C) with the ratio

$$\frac{3F_2^p + 4F_2^n}{F_2^p}, \tag{27}$$

which is (in a sense) the inverse of the "dilution factor" for the polarized proton in ^{7}Li. The corresponding ratio then becomes

$$R_2 = \frac{3F_2^p + 4F_2^n}{F_2^p} \frac{A_{||\ ^7\mathrm{Li}}}{A_{||\ p}} = \frac{g_{1^7\mathrm{Li}}^z + \frac{P_{zzz}}{P_z} g_{1^7\mathrm{Li}}^{zzz} + C_{^7\mathrm{Li}}(A_2)}{g_1^p + C_p(A_2)} \frac{3F_2^p + 4F_2^n}{F_{2A}^0 + \frac{1}{2} P_{zz} F_{2A}^{zz}}. \tag{28}$$

Again, we assume that the asymmetries have already been corrected for target polarization. Equation 28 shows that this ratio is somewhat complementary to R_1, in that it cancels out the contribution to the polarized EMC effect that comes from the **un**polarized structure function ratios which enter the usual, unpolarized EMC effect. Ratio R_2 is therefore a more direct measure of the *additional* binding effects due to polarization degrees of freedom, beyond the standard EMC effect that is already well-known.

D. Polarized EMC effect : Models

In the following, we discuss several recent models of the polarized EMC effect, which can be compared to the data we propose to collect. In all cases, we show the ratio R_{pol} defined in Eq. 23. In Section II C, we show how these models translate into predictions for the measured quantities R_1 and R_2, Eqs. 26−28. We note that in an "extreme" nucleons-only model, where ^{7}Li consists simply out of 3 free protons and 4 free neutrons at rest, by definition the ratio $R_{pol} = 1$. Any deviation from unity can therefore be termed a "nuclear binding effect".

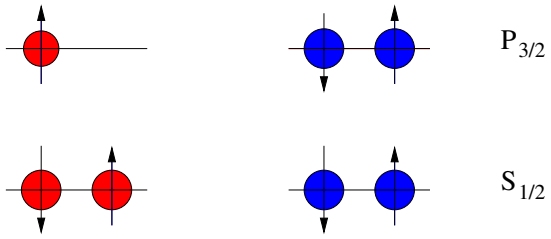

FIG. 2. Structure of ^{7}Li in a simple shell model picture. Protons are red and neutrons blue.

1. *Naïve Nuclear Model*

The first step towards a more realistic nuclear model is to incorporate the fact that the average polarization of nucleons inside a nucleus is not equal to that of the nucleus overall. In the case of ^{7}Li, which has total angular momentum $S = 3/2$, the nuclear shell model predicts that 2 protons and 2 neutrons are in the 1s shell with total angular momentum zero, while the spin quantum numbers of the nucleus are carried by the two neutrons and one proton in the $1p_{3/2}$ shell (see Fig. 2). Naïvely, one might expect the two neutrons to couple to total angular momentum zero (because of the Pauli principle), which means that a single $1p_{3/2}$ proton would carry the entire nuclear spin. A standard shell model calculation [40] finds that there is some non-zero probability for the neutrons to couple to angular momentum $J > 0$, and yields a proton polarization (or, rather, an expectation value for the z-component of the spin, summed over all protons) of $P_p = 13/15 \approx 0.867$ and for the neutrons, $P_n = 2/15 \approx 0.133$. More recent, state-of-the art microscopic calculations [41] yield a nearly identical result for the proton polarization, $P_p = 0.866$, but a much smaller (and slightly negative) expectation value for the neutron spin, $P_n = -0.037$. Ignoring all other nuclear effects, we arrive at the "naïve nuclear model" prediction

$$R_{pol}^{NNM} = 0.866 - 0.037\frac{g_1^n}{g_1^p}. \tag{29}$$

2. *Standard Nuclear Model*

For a complete prediction of the various ratios defined in the previous section within in the context of "standard nucleon-only nuclear physics", one needs the following ingredients:

1. A realistic wave function model for the nucleus in question, which can predict the probability of finding a nucleon of type N (neutron or proton) with three-momentum $\vec{p}$ relative to the quantization (z-) axis, as well as the polarization $\vec{P}(\vec{p})$ carried by that nucleon, for each possible magnetic substate m_S of the nuclear spin.
2. Parametrizations of the nucleon unpolarized ($F_1^N(x,Q^2)$, $F_2^N(x,Q^2)$) and spin structure functions $g_1^N(x,Q^2)$, $g_2^N(x,Q^2)$ or alternatively the asymmetries $A_1^N(x,Q^2)$, $A_2^N(x,Q^2)$.
3. A convolution prescription on how to generate the nuclear structure functions defined in the previous section from the above ingredients.
4. Potentially an interaction model that includes the effects of final state interactions.

Such a model will be crucial as a benchmark to which we can compare the results of the proposed experiment. Any deviation from the expectations of this model could be properly interpreted as a "genuine EMC-type effect" in the polarized structure functions. At present, most of these ingredients are either already available, or very close to what will be needed for this program. In particular, the status for each of the 4 ingredients above can be summarized as follows:

1. Recently, the properties of few-body nuclei have been modeled with unprecedented accuracy from first principles, using realistic nucleon-nucleon potentials, three-body forces and sophisticated numerical methods like Greens Function Monte Carlo (GFMC) [42]; for an example see Fig. 3. These and related methods (Variational Monte Carlo) can be used for the purpose described above. A recent publication [41] provides realistic nucleon momentum distributions in light nuclei, including ^{7}Li, for each nucleon type and polarization direction separately. We are using a simple implementation of the numerical tables provided by the authors for the purpose

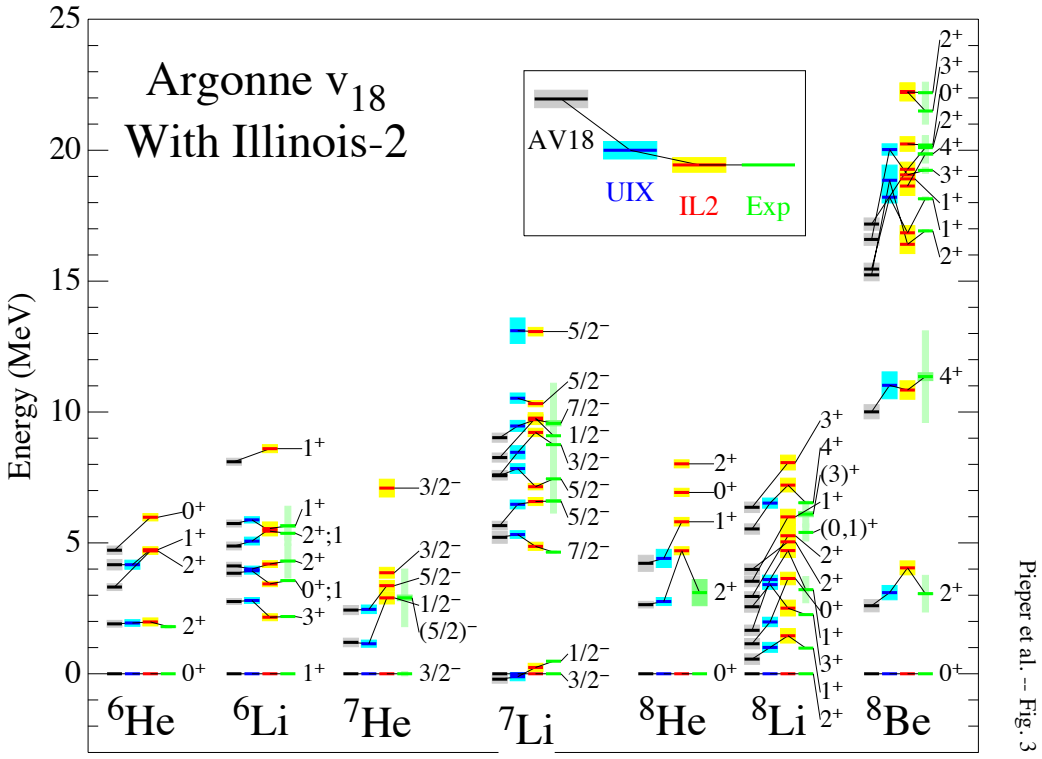

FIG. 3. Green's Function Monte Carlo (GFMC) calculations for ground states and excited states in the $A = 6 - 8$ region from [42]. This figure illustrates the precision achieved in modern few-body nuclear structure calculations. Typical deviation from experimental values (where available) are of order 100 keV or less.

of this proposal; however, it must be stressed that a complete model with all the necessary information should be available from these authors (who are collaborators on this proposal) by the time the experiment is likely to take place.

2. All of the polarized and unpolarized structure functions of both nucleons have been measured with great accuracy in all three Halls during the 6 GeV era of Jefferson Lab. Several detailed phenomenological fits to these structure functions exist and are actively maintained, both by members of the group on this proposal and by others [43–45]. Once data at 12 GeV become available, they will be incorporated into these fits. The kinematic coverage of these data overlaps completely the kinematics of the proposed experiment. A shown in Section II D, the various ratios discussed in the previous section are not very sensitive to the spin structure function models; our knowledge of all structure functions will be more than adequate for the present purpose.

3. Several approaches for the folding of nucleon momentum distributions with polarized and unpolarized structure functions exist, see for instance [46]. For this proposal, we used a Monte Carlo approach, where we loop over all nucleons in the nucleus, picking their momenta at random from the underlying probability distrtibution [41]. We calculate the full polarized cross section in the rest frame of that nucleon, and boost the resulting scattered electron back into the lab frame. We assume an "off-shell energy" of the struck nucleon of $E^* = M_N - 5.5$ MeV, where 5.5 MeV is the average nucleon binding energy in ^{7}Li. This simulation software has been used for other purposes, e.g. for one of the parallel analyses of the BONuS experiment, with good results [47]. (The results are shown by the purple and blue lines in Fig. 4.) We also use a variant of this Monte Carlo generator, where the active nucleon is initially on-shell, which violates energy-momentum conservation but makes the treatment more straightforward (orange curve).

   As a consequence of our treatment of off-shell kinematics, a modest "EMC-like" effect appears already in the unpolarized cross section ratios of nuclear to nucleon targets, corresponding to an "effective $x-$rescaling" by an average of about $\eta = 1.02$. For the final comparison with experimental results, we will use more rigorous

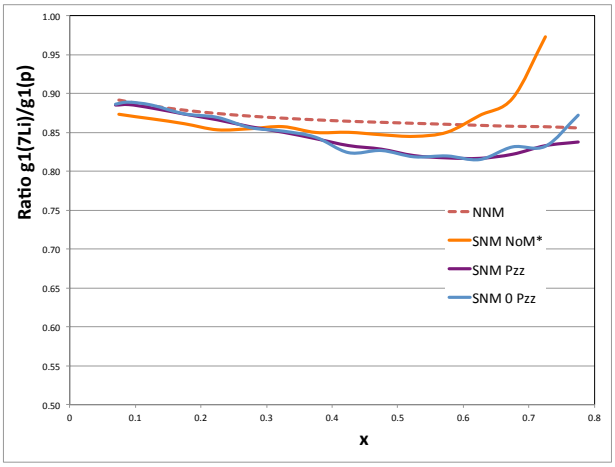

FIG. 4. Predictions for the ratio R_{pol} for both the naïve nuclear model (red dashed line) and the standard nuclear model (purple and light blue lines), implemented as described in the text. We also show results from the same Monte Carlo generator with nucleons that are initially on-shell (ignoring all binding effects – solid orange line). The blue line assumes a target with zero tensor polarization $P_{zz} = P_{zzz} = 0$, while the purple and orange lines include the effects of experimentally realistic values of $P_{zz} = 0.54, P_{zzz} = 0.11$. The slight fluctuations around a smooth curve are due to Monte Carlo statistics and don't have any physical meaning.

prescriptions for the treatment of off-shell effects. It is important to note that the momentum p of the $1p_{3/2}$ proton that carries most of the nuclear polarization is mostly below 300 MeV/c, meaning that its "off-shell mass" $M^* = \sqrt{E^{*2} - p^2}$ is within 4% of its on-shell mass on average.

4. Recently [48], it has been pointed out that even in inclusive scattering off few-body nuclear targets, final state interactions may slightly modify the cross section from convolution model expectations. We will work with the authors of [48] to implement state-of-the-art final state interaction calculations in the standard nuclear model predictions.

As an illustration of our present implementation of the "standard nuclear model" (SNM), we show in Fig. 4 the results for the polarized EMC ratio R_{pol} (Eq. 23) from both the simple Eq. 29 (dashed red line) and from our convolution model described above. The "on-shell version" (orange line), which includes only the effects of Fermi motion and effective polarization but no binding effects, is close to but slightly below the "naïve nuclear model" (dashed red line) except for a rise at high x, as expected. (The slight reduction is a consequence of ignoring binding effects, which makes the average "effective" x smaller than the measured one; this combines with the fact that the asymmetry is a monotonically rising function of x). Including binding effect by assuming an average off-shell energy $E^* = M_N - 5.5$ MeV for the struck nucleon, the expected ratio changes visibly (purple and blue lines), even without assuming modified quark distributions. These deviations are at most 5% from the naïve ansatz, similar to the effect of "standard nuclear binding" on the unpolarized EMC ratio.

For a realistic prediction of the polarized EMC effect within some of the "genuine EMC-effect" models discussed in the following, we would need to combine the correct convolution with realistic nuclear wave functions and the modified quark distribution functions predicted by these models. In any case, we expect the nuclear model uncertainties to be significantly lower than 5% over nearly the whole measured x-range by the time of the anticipated experiment.

Figure 4 also shows that, within standard nuclear physics, tensor polarization of the target plays a very minor role. The blue curve shows the result without tensor polarization (which is not experimentally feasible), while the purple curve includes realistic tensor polarizations. As one can see, the difference is negligible over nearly the whole measured range (small deviations are most likely due to Monte Carlo and model uncertainties), possibly with the exception of the highest x point.

3. Rescaling Models

A very recent publication [30] contains predictions from two models for the EMC effect. The first model employs a rescaling of the Bjorken variable, x, which is replaced with $x^* = \eta x$ when the bound nucleon structure functions

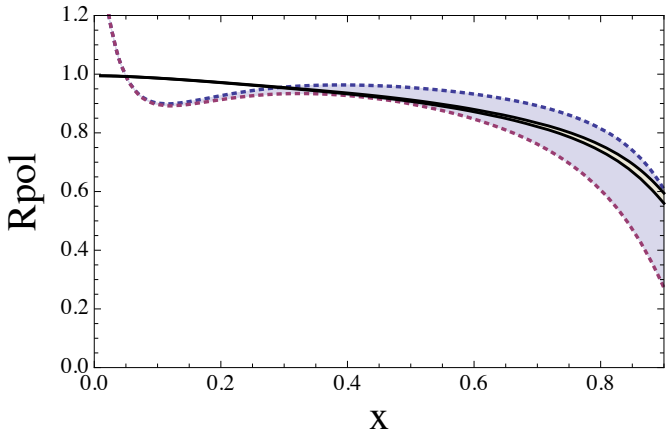

FIG. 5. Predictions for the ratio R_{pol} (Eq. 23) for the "MSS" model of Ref. [30]. The shaded band with dotted edges corresponds to their range of parameters for the contribution of sea quarks to the ratio and the corresponding rescaling of x for the valence quarks. The narrow band with solid edges corresponds to the unpolarized EMC effect in the same model, which is similar in magnitude to the polarized effect when only $x-$rescaling is considered. Note that both curves would have to be convoluted with a realistic (polarized) nucleon momentum distribution, as described in the previous section, to be directly comparable to our definition of R_{pol}.

are evaluated. A good fit to the unpolarized EMC data is obtained with $\eta = 1.011$, while for the polarized case the authors consider values between $1.01 \leq \eta \leq 1.02$. Depending on the exact choice, the polarized EMC effect can lead to a more than 10% reduction of the nuclear spin structure function around $x = 0.7$, although the effect is not much different from that in the unpolarized case. The resulting prediction for R_{pol} is similar to our result for the "standard nuclear model" including off-shell effects; see the blue and green curves in Fig. 4 (corresponding to $\eta \approx 1.02$).

The second model (the so-called "modified sea scheme", MSS) assumes an enhancement of the pion cloud contribution to the nucleus, and a corresponding reduction of the momentum fraction carried by valence quarks (leading again to x-rescaling). This approach leads to a considerable enhancement in the region around $x \leq 0.1$, which is not visible in the unpolarized EMC ratio, since the latter is traditionally formed relative to the *deuteron*, which in this model also contains a significant pion cloud enhancement. However, for the polarized case, the comparison is with the free proton structure function g_1, which yields to a significant and observable rise of the ratio R_{pol} at low x, see Fig. 5. Interestingly, the magnitude of this effect is not dissimilar to that in the calculation within the Chiral Soliton Model and the approach by Guzey and Strikman, which we discuss further below.

4. Thermodynamic Bag Model

The authors of Ref. [29] have developed a thermodynamic description of nucleon structure functions in terms of bag model parameters, finite temperatures and chemical potentials for the various quark flavors. Their model agrees well with experimental data on nucleon spin structure functions and fulfills the Bjorken sum rule.

They use this model, together with a simple convolution within a Fermi gas model of the nucleus, to predict the polarized quark distributions in ^{7}Li and ^{27}Al. They find a reduction of both up and down PDFs Δq over the range $0 < x \leq 0.8$ with a maximum depletion of maybe 3-4% at $x = 0.6$ and a rise beyond that due to Fermi motion. This leads to a slightly larger decrease in the polarized EMC ratio relative to the unpolarized one for nearly all x. Qualitatively, their prediction for ^{7}Li looks quite similar to the one discussed in the next section, although overall the EMC effect in this model is much weaker (also in the unpolarized sector).

5. Quark-Meson Coupling Model

One approach to model both nucleon and nuclear structure functions consistently is based on a variant of the Quark-Meson Coupling model (QMC), namely the relativistically covariant Nambu-Jona-Lasinio model, where the nucleon is described as a quark-diquark bound state (see Ref. [49] and references therein). Nuclear binding in this model occurs through direct quark interaction with a scalar and vector mean field, which in turn modifies quark

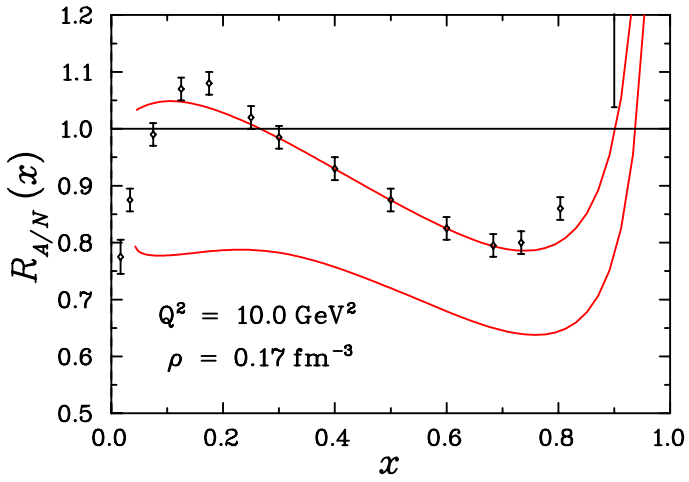

FIG. 6. Predictions for both the unpolarized (upper line) and the polarized (lower line) EMC effect, in the limit of nuclear matter [49]. The data are well described above the shadowing region. Obviously, the polarized EMC effect is significantly stronger than the unpolarized one in this model, and leads to a uniform depletion of the EMC ratio.

distributions inside the nucleon leading to a self-consistent and numerically accurate description of the (unpolarized) EMC effect (see Fig. 6) as well as nuclear matter properties. As a reaction to the presence of the scalar field, the lower components of the valence quark wave functions are enhanced. Since spin structure functions are particularly sensitive to these lower components, the EMC effect is magnified for g_1 relative to F_1, leading to the significantly stronger deviation from unity for the polarized EMC ratio in Fig. 6. It should be mentioned that this model does not include sea quarks explicitly, which instead are introduced by DGLAP evolution from the low model scale $Q_0^2 = 0.16$ GeV^2 to the Q^2 of the measurement.

The authors of Ref [49], who are collaborators on this proposal, have applied this model to finite nuclei, as well [25]. In the case of ^{7}Li, the enhancement of the EMC effect for polarized quark distributions is somewhat countered by the fact that the $1p_{3/2}$ proton carrying most of the nuclear polarization experiences less of the scalar and vector mean fields, due to its greater spatial range. Nevertheless, this model predicts a significant polarized EMC effect for ^{7}Li, which deviates significantly in its $x-$dependence from the unpolarized EMC ratio. In Fig. 7 we show the exact result expected for the ratio R_{pol} as defined in Eq. 23, as well as the "naïve nuclear model" (NNM) curve (see above). We also show the effect from a small contribution by the tensor spin structure function $g_{1^7\mathrm{Li}}^{zzz}$ due to the expected tensor polarization of the target. This figure demonstrates a deviation from the NNM by as much as 10% over a large range in x, and a non-trivial $x-$dependence of the ratio R_{pol}, which we will be able to measure with high statistical significance (see Section II C).

6. Chiral Quark Soliton Model

A somewhat related approach to calculating polarized nuclear structure functions uses the Chiral Quark Soliton Model (CQS) in the large-N_C limit as another relativistic mean field approximation for baryon structure [27]. This model has the advantage that it includes antiquark degrees of freedom and quark and antiquark orbital angular momentum explicitly, and it also leads to a good description of the unpolarized EMC effect.

In Fig. 8, we show the results of this calculation for polarized quark distributions in nuclear matter, evolved to a scale $Q^2 = 10$ GeV^2. The thin curve in this figure is the effect due to valence quark effects alone - it can be seen that it is in rough agreement with Fig. 6, which shows that these two approaches arrive at similar results for valence quarks. However, the authors stress that there is a strong modification of this result due to the influence of sea quarks, which leads to a reduction of the polarized EMC effect at moderate x and a strong enhancement of the ratio, beyond unity, at $x \leq 0.3$. This enhancement is in strong contrast to the **un**polarized EMC effect, which shows only little enhancement due to sea quarks. It is in qualitative agreement with the MSS model discussed above, and the shadowing argument explained in the next section. While the prediction in Fig. 8 is for nuclear matter (and contains several approximations), it is clear that for finite nuclei, similar sea quark effects should be present and lead to a significant modification of the $x-$dependence of the ratio R_{pol}.

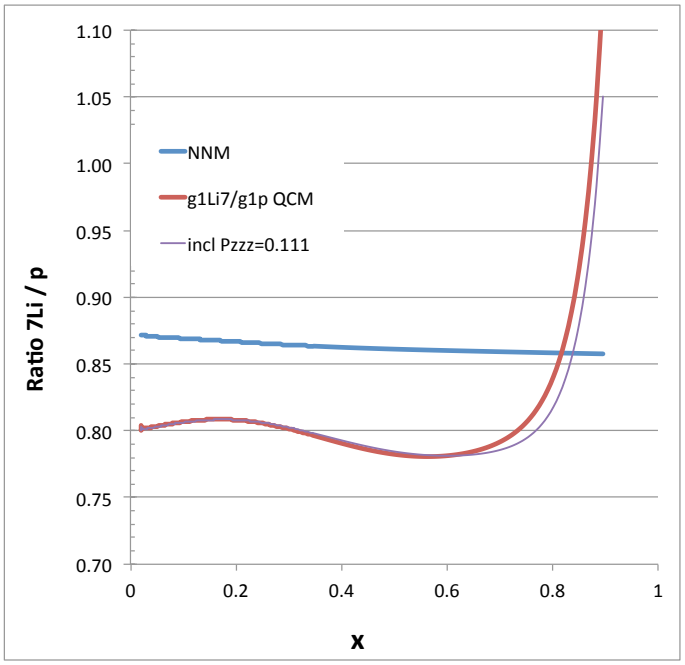

FIG. 7. Predictions for the ratio R_{pol} for the QMC model of Ref. [25]. The solid blue line corresponds again to the NNM prediction, while the red line shows the full model prediction for zero tensor polarization. Including the experimentally expected $P_{zzz} \approx 0.11$ yields the thin purple line, which contains all nuclear effects related to the structure function $g_{1^7\mathrm{Li}}^{zzz}$.

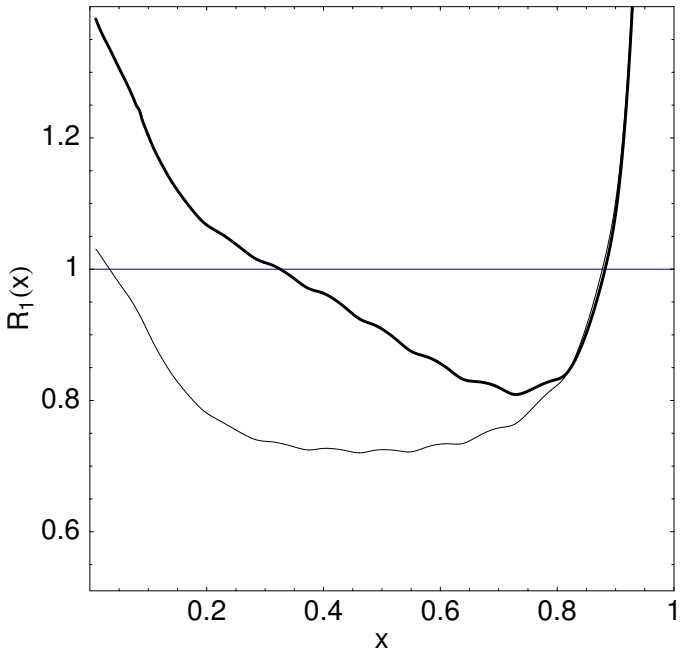

FIG. 8. Predictions for the ratio R_{pol} from Ref. [27]. The curves are for nuclear matter, assuming 100% nucleon polarization and $Q^2 = 10$ GeV^2. The thin curve is due to valence quarks only, while the heavy curve includes the full result for both valence and sea quarks.

7. *Shadowing Model*

In the paper by Guzey and Strikman [28], the authors focus on the EMC effect at small to moderate x, $10^{-(4-5)} < x \leq 0.2 - 0.25$. The very low x region is modified in nuclei by shadowing, which is essentially the consequence of coherent scattering from more than one nucleon. Shadowing has been clearly observed and is a relatively well-understood part of the overall EMC effect. The authors state that this effect is roughly doubled in size for *polarized* EMC ratios in light nuclei due to combinatorics – the interference leading to shadowing involves only nucleon pairs which include the one nucleon that carries most of the polarization (the $1p_{3/2}$ proton in the case of ^{7}Li), while in the unpolarized case, all possible combinations of any two nucleons contribute which dilutes the effect.

A detailed theoretical calculation finds that the non-singlet part of the spin structure function g_1 (see below) is reduced by as much as 16% at $x = 0.01$ and about 10% at $x = 0.05$ because of shadowing, beyond the reduction due to the "effective nucleon polarization" in ^{7}Li. Fermi motion and other binding effects play a very small role at these low x. We note that most of the shadowing region is outside the reach of Jefferson Lab, even at 11 GeV beam energy, and this prediction will ultimately have to be checked by a electron-light ion collider. However, if shadowing persists until $x = 0.05$, we will certainly be able to see the downturn of the ratio R_{pol} predicted by this model. More importantly, the authors predict a dramatic *increase* of this ratio beyond $x = 0.05 - 0.1$, which is well within the acceptance of the proposed experiment.

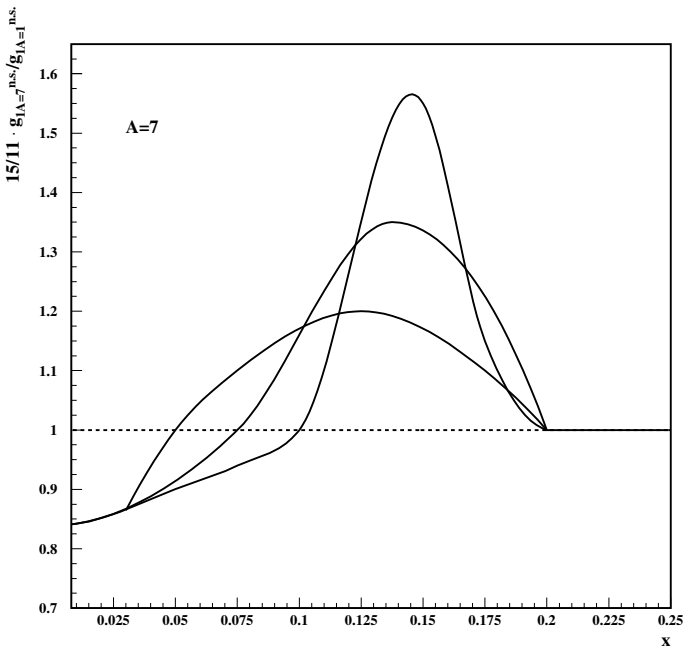

FIG. 9. Predictions for the ratio R_{pol} (for the non-singlet part of the spin structure functions) at low to moderate x, following the model by Guzey and Strikman [28]. The curves shown are for several different scenarios considered by the authors, and are relative to the prediction of the "naïve nuclear model" (meaning they would have to be multiplied by roughly 0.9 to agree with our definition of R_{pol}). The ratio is suppressed significantly below $x = 0.03 - 0.1$ due to shadowing, which is compensated by a strong enhancement at higher x.

This enhancement is due to the requirement to fulfill the Bjorken sum rule, which relates the integral over the isospin triplet structure function for any isospin doublet (nucleon or nuclear) to the axial beta-decay constant g_A for that doublet. The authors assume a shape of the enhancement similar to that observed in the original EMC effect measurements (Fig. 1), but vary the cross-over point between $x = 0.05$ and $x = 0.1$. In each case, the enhancement is modeled to compensate the reduction in the shadowing region, to keep the integral equal to unity. Therefore, the increase of R_{pol} above the "naïve nuclear model" expectation is driven by the location of the cross-over point, and could be anywhere between 20% (low crossover) and 55% (crossover at $x = 0.1$). The resulting curves for the polarized structure function ratio are shown in Fig. 9. We note that this dramatic enhancement is in qualitative agreement with other models discussed above, in particular the "MSS" model by Fanchiotti et al. [30] and the CQS model by Smith and Miller [27].

This model is specifically formulated for the non-singlet (isospin-triplet, Δq_3) part of the spin structure function g_1 (to be able to invoke the Bjorken Sum Rule), which would involve a comparison of the difference between ^{7}Li and

the (radioactive) nucleus ^{7}Be to the difference $g_1^p - g_1^n$. We observe that the proton structure function g_1^p can be decomposed as follows [50]:

$$g_1^p = \frac{1}{18}\left(\frac{3}{2}\Delta q_3 + \frac{1}{2}\Delta q_8 + 2\Delta\Sigma\right) \tag{30}$$

in leading order, where Δq_8 is the SU(3) octet part (non-singlet as well) and $\Delta\Sigma$ is the singlet contribution. (At NLO, the gluon distribution $\Delta G(x)$ mixes with the singlet part.) The authors of Ref. [28] calculate the shadowing effect for the ratio ^{7}Li over proton directly (with some further assumptions about the singlet contribution) and find an even stronger deviation from the "naïve nuclear model" (see their Fig. 2). While any depletion of the singlet contribution does not have to be compensated by a corresponding enhancement at higher x (within their model), it seems reasonable to assume that more than 50% of the predicted enhancement should translate to the ratio R_{pol} including the singlet. This would translate into an enhancement of between 10% and over 30% for R_{pol} in the region $0.1 \leq x \leq 0.2$.

8. Model Summary

In summary, nearly all models available at this time predict a reduction of R_{pol} beyond that due to the less than 100% polarization of the proton in ^{7}Li. In most models, this effect is stronger than in the corresponding unpolarized EMC ratio, or has a strikingly different $x-$dependence. This means that the polarized EMC effect will be apparent not only in the ratio of structure functions g_1, but also in the corresponding asymmetries, e.g. the ratio R_2 defined in the previous section.

The main difference between the various models is whether they predict a more-or-less uniform depletion for all x, as for instance in the QMC model, or a strong enhancement at lower $x \leq 0.2$, as in several of the other models discussed. Therefore, it is the full $x-$dependence of the various ratios defined above that will provide crucial information to discriminate between these various models, many of which do a similarly good job describing the **un**polarized EMC effect. Of course, a measurement of this dependence, as proposed here, may well show results not foreseen by any of the models discussed, in a sense repeating the surprise of the original measurement by the EMC.

II. EXPERIMENT

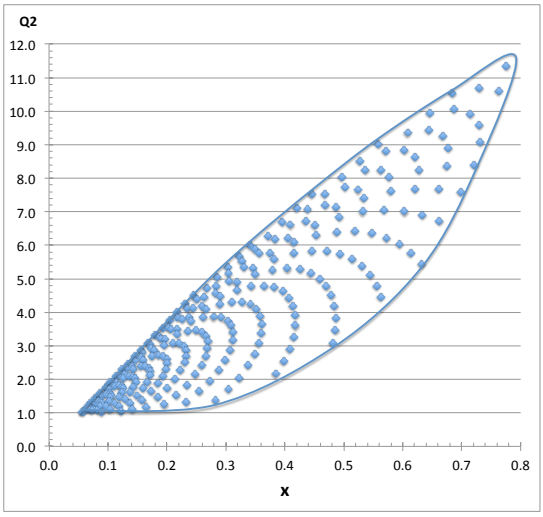

FIG. 10. Kinematic acceptance of the proposed experiment.

In the following, we will discuss the details of the proposed experiment and present the expected results with statistical and systematic uncertainties. We assume 50 days of data taking as specified below, and a luminosity of 2×10^{35} e^-/s $\times$ nucleons/cm^2, consistent with the expected performance of CLAS12. Figure 10 shows the kinematic coverage for the experiment, which is the same as for the approved inclusive structure function program for the proton and the deuteron with CLAS12 [51]. We used the package "FASTMC" for this and several other simulations displayed in this section.

A. Polarized Target

1. *Target Material*

As explained in the previous section, we have chosen ^{7}Li as a nucleus which should exhibit a sizable EMC effect yet is small enough to yield a relatively large asymmetry and to be amenable to precise microscopic calculation. As it turns out, Lithium isotopes are also among the few nuclei which have been successfully polarized to a high degree in the past.

Since pure, metallic ^{7}Li is not suitable for a target polarized by Dynamic Nuclear Polarization (DNP) because it cannot be penetrated by microwave radiation, we have to use a non-conducting compound. The best option (for which the most experience exists) combines lithium with hydrogen to form lithium hydride, in a ratio of 1:1. However, we would like to avoid (as much as possible) the need to subtract the confounding contribution from free protons from the measured asymmetry on ^{7}Li; therefore, we propose to use deuterium as the partner in this compound, i.e. ^{7}LiD as our target material. This material is chemically and physically very similar to ^{6}LiD, which has been successfully used both by the COMPASS collaboration [52–54] and by E155 at SLAC [55, 56].

In particular the COMPASS collaboration [53] has developed a mass production scheme which ensured the production of 0.5 kg of ^{6}LiD, starting from highly enriched ^{6}Li and D_2 gas. For the proposed experiment, substantially smaller quantities (of the order of maybe 20 g) of both ^{7}LiD and ^{6}LiH will be needed (see below), which should not pose any serious obstacles; pure Lithium-6 isotopes and ^{6}LiH can be obtained from ORNL. We have also identified at least one commercial supplier for ^{7}LiD with an isotopic purity of at least 98%. The material will be cut into small "beads" of a few mm in size, which can be immersed in the liquid ^{4}He coolant of the standard CLAS12 polarized target. To introduce the necessary paramagnetic centers, the material will have to be irradiated with a dose of about $2 \times 10^{17} e^-$/cm^2 at 190 K temperature. There are several options for this (including the injector test stand presently

being installed at Jefferson Lab); in any case, the experience of the COMPASS collaboration will provide valuable guidance.

2. *Target configuration*

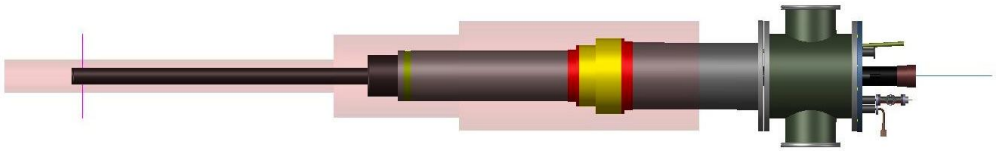

FIG. 11. Conceptual design for the CLAS12 longitudinally polarized target.

For the proposed experiment, we will use the longitudinally polarized proton/deuteron target presently under development for CLAS12 (Fig. 11), with no major modifications. This target has been partially built with funding from the NSF MRI program by a collaboration of several institutions, most of which are part of this proposal. At present, all the major (expensive) parts of the target are in hand; the final integration of these parts into an operating target, with strong involvement of the Jefferson Lab target group, will begin in time for the approved CLAS12 longitudinal spin program [51].

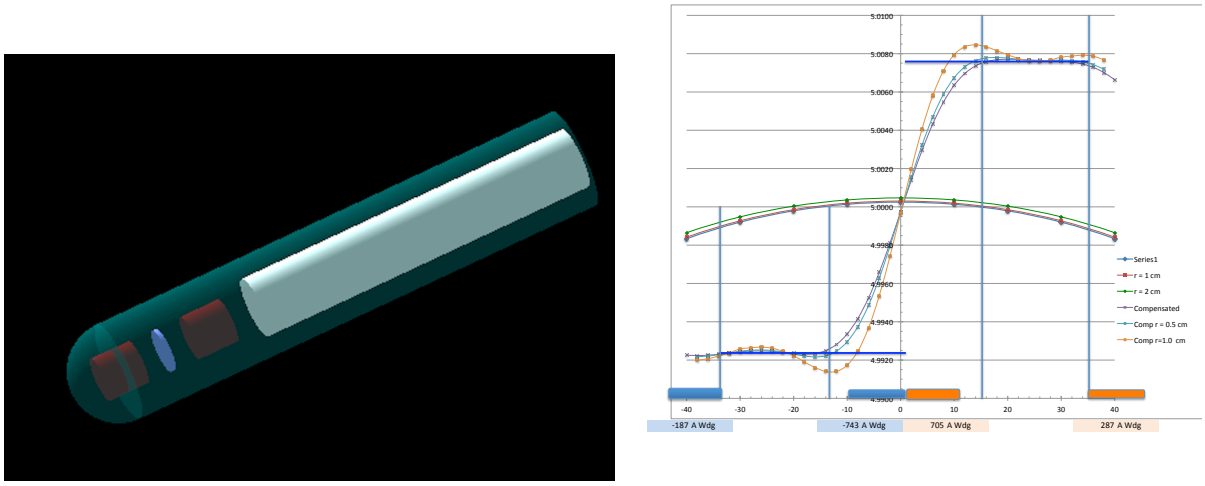

FIG. 12. LEFT: GEANT4 implementation of the two target cells for the CLAS12 longitudinal target. The white volume to the right is the beam line vacuum tube, and the cyan shade indicates liquid Helium coolant. RIGHT: Preliminary results of a study for superconducting compensation coils to achieve opposite target polarization in two cells with the same microwave frequency. The nominal target fields required are indicated by the blue horizontal bars, while the uncompensated target field is indicated by the smooth curves in the center and the compensated field (at different radial distance from the beam line) by the three remaining curves.

Several of the collaborators on this proposal are presently working on the details of the actual target chamber for this program, which will contain the target material, the liquid Helium coolant, and all the necessary instrumentation for microwave irradiation, NMR and thermometry as well as target anneals. Independent from the present proposal, it turns out that it would be advantageous to have *two* target cells, which are both traversed by the beam in sequence. This is mostly for the benefit for the large program of concurrent measurements approved for the CLAS12 polarized target that aim to measure single target spin asymmetries (TSA) on the proton and the deuteron (both for Deeply Virtual Compton Scattering and Transverse Momentum Dependent PDF measurements). The reasons are the same as in the case of the COMPASS target, which also entails (at least) two target cells [53]: the target polarization can not be reversed very rapidly (and therefore not very often), and systematic errors due to time-dependent detector efficiencies and luminosity must be kept small using other methods. By having two targets with opposite polarization (which are both reversed on a regular basis), one can essentially obtain two independent measurements of the same

quantity (TSA), with largely opposite systematic effects. The groups at UTFSM and ODU have embarked on a detailed modeling of this "two-cell solution", including a full implementation in the CLAS12 simulation code GEMC and a design for a superconducting compensation coil that allows the simultaneous polarization with opposite sign of two target samples using the *same* microwave frequency; see Fig. 12. We note that we will not use this particular feature (opposite target polarization) during the proposed experiment, since, for a double polarization measurement, systematic effects from detector drifts etc. can be kept minuscule by the standard method of rapid beam spin reversal. However, the presence of correction coils also allows us to compensate for any inhomogeneities in the magnetic field produced by the CLAS12 central solenoid. At present, the design foresees two cells of diameter 2 cm and length 2 cm, separated by 2.8 cm (of liquid Helium).

Instead, we will fill the second target cell with ^{6}LiH or possibly $^14NH_3$, allowing us to measure the asymmetry for both ^{7}Li and the proton simultaneously, with the same apparatus, thereby minimizing systematic effects in the EMC ratios. To further enhance this advantage, we will also exchange the two target materials roughly halfway through the experiment, which again will yield two nearly independent measurements of the EMC ratios, with largely opposite systematic errors. We chose ^{6}LiH for the reference material to mimic, as closely as possible, the physical and spin-properties of the ^{7}LiD target including the packing fraction and dilution factor; both compounds are composed of a highly polarized "proton-like" component and a much less polarized spin-1, "deuteron-like" component. However, we plan to continue detailed studies of the relative advantages of this choice over the "standard" NH_3 proton targets, and will decide which of these gives the best trade-off in terms of statistical and systematic uncertainties. In any case, the magnetic moments of all species under consideration (except N) are very close, and the same NMR circuits used for proton and deuteron measurements will be fully adequate for the proposed experiment.

3. Expected Operational Parameters

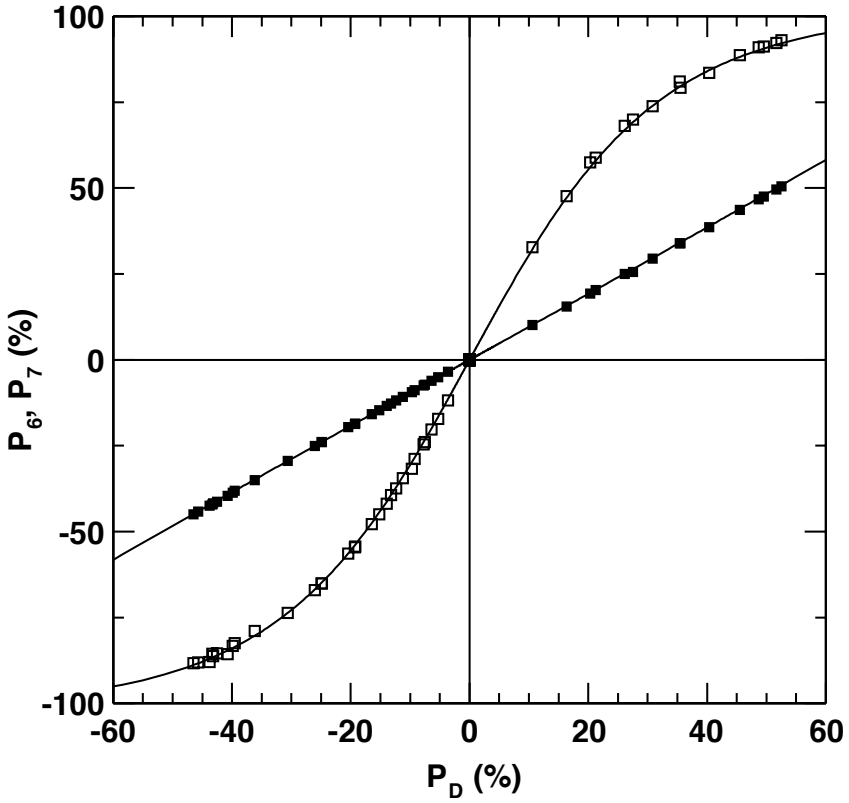

FIG. 13. Relationship between the measured polarizations of various target species (open symbols for ^{7}Li and black squares for ^{6}Li), as found by the COMPASS collaboration [53]. The prediction by the EST concept is shown by solid lines, which describe the data extremely well.

The magnetic hyperfine splitting between neighboring polarization states of Lithium-7 is fairly similar to that of

the proton, with an "effective" magnetic moment of 2.17 μ_N vs. 2.79 μ_N. For this reason, most of the equipment and procedures used to polarize ^{7}Li are very similar to those for a proton target, with some notable exceptions. We assume a longitudinal magnetic field of 5 Tesla (provided by the CLAS12 central solenoid) and a microwave system at 140 GHz with up to 1 W delivered to the target. We assume a target temperature close to 1 K, which is the design value for the evaporation refrigerator being built for CLAS12. Under similar conditions, proton polarizations of over 90% have been achieved in the lab, and about 85% in a recent experiment in Hall A (g2p) under beam exposure. With CLAS12, we will have the advantage that we can run with relatively low beam currents (of order 15 nA), as well as smaller sample sizes (maybe 4 g per target cell), which will require significantly lower microwave power (and therefore less target heating). Using Equal Spin Temperature (EST) to predict the polarization of ^{7}Li, we find that the somewhat lower "effective magnetic moment" translates the proton values to 65% - 80%. This is a realistic prediction, since COMPASS [53] found that EST works very well in the case of lithium hydrides, see Fig. 13.

With a 2.5 T field and up to 300 mK in their dilution refrigerator, COMPASS achieved a deuteron and ^{6}Li polarization of about 50% after several days, and 40% within 1 day. Their measured value for the ^{7}Li polarization exceeded 90% (see Fig. 13). Their ratio of B/T is within a factor 2 of that expected for the present experiment, which again is consistent with a somewhat lower polarization for ^{7}Li in the range indicated above. For the purpose of this proposal, we assume a polarization of $P_z = 0.8$, which is at the upper end of the expected range. However, we use conservative estimates for the acceptable luminosity and dilution factors, which would have to be improved by only 15-30% to achieve the same statistical precision for the lower polarization. In any case, our results show that a 15% increase of our statistical error bars will worsen the significance of the proposed measurement only moderately.

Assuming $P_z = 0.8$ and EST, we predict for the tensor polarizations $P_{zz} = 0.55$ and $P_{zzz} = 0.11$. These values would become significantly smaller (0.42/0.07) at the lower end of the expected range. At the same time, the D part of the compound would be polarized to about $P_z = 0.36, P_{zz} = 0.10$. Similarly, with the proton polarized to $P_z = 0.85$, the ^{6}Li in the second target cell is expected to have a polarization of only 0.24 and negligible tensor polarization. Keeping in mind the "effective deuteron polarization" in ^{6}Li of about 0.87, we see that the polarized ^{6}Li in our proton reference target partially compensates for the polarized deuteron in our primary target. Nevertheless, we will use a complete model of deuteron spin structure functions to correct for this "polarized contamination" in both targets; given the smaller size of both the polarization and these structure functions relative to the "proton-like" ones, this will be a moderate correction with small systematic uncertainties.

We will measure the target polarization using the standard (proton) NMR circuits and the "area method" (different from deuterium, lithium isotopes do not show much broadening or several peaks in the NMR signal). The NMR circuits of both target cells will be calibrated using the signal at thermodynamic equilibrium (TE), i.e. without microwave irradiation turned on. One advantage of exchanging the target material (while keeping the NMR circuits unchanged) will be that we can cross-check this calibration. We also will use a second, completely independent method to ascertain the polarization of both targets, see Section II B.

One difference between lithium hydrides and other typical polarized target materials (e.g., ammonia) is the longer relaxation (and polarization) time required. As stated above, it took about 1 day to reach about 80% of the maximum possible polarization, and this polarization kept rising for as much as a week in the experience of COMPASS. On the other hand, lithium hydrides are extremely radiation resistant, which means we won't have to exchange the target material (at least not often). In fact, there are indications that both the speed of the polarization build-up and the ultimately achievable polarization improve further with additional irradiation at the 1 K temperature of standard operation. We may also be able to reduce the number of required anneals to maybe one a week. Therefore, our collaboration will very carefully optimize all procedures connected to the polarized target, to maximize the effective product of target polarization (squared) and beam on target. For instance, we will try to combine an anneal (which should destroy the target polarization to a good extent), a TE measurement, and repolarization with the *opposite* target polarization of both cells on days where beam is not available for other reasons, e.g. regularly scheduled accelerator maintenance days. During longer shutdowns, as well as before and after the experiment, longer TE measurements can be scheduled to increase the precision of the calibration. As stated above, at least once during the experiment, we will exchange the target material between the two cells, to further reduce systematic uncertainties, again most likely during a longer shutdown. In spite of these expected synergies, we are asking for 5 additional days to guarantee that we have enough time for the initial determination of optimum target parameters with beam and for any necessary interruptions (changes of target material, anneals etc.) during the experiment.

Finally, we would like to state that several of us are embarking on an extended R&D effort to verify some of the parameters mentioned above. Both the group at UTFSM and the present CLAS12 longitudinally polarized target collaboration are exploring options to use simulations as well as to set up target test stands where we can study optimum microwave irradiation, heat transport away from the target, magnetic field compensation coils, and the properties of the foreseen target material. These efforts, for which some of us are pursuing significant new funding, will clearly be strengthened if the present proposal is approved with sufficient priority. With previously tested target material in hand, the amount of time required to set up and optimize the polarized target inside CLAS12 will be

only one or two weeks (without beam). We expect that the present experiment, if approved, will be scheduled in conjunction with the other longitudinally polarized target experiments, minimizing this overhead for both. We did not include these "no beam" days in our beam time request.

B. Experimental Details

Apart from the polarized target, this experiment will use CLAS12 in its standard configuration without modifications. In particular, we do not *require* the presence of the RICH planned for CLAS12, although other experiments that might run in parallel with this one could require it. We do expect the full complement of forward and central detectors to be present (the nTOF is optional), in particular we need the forward micromega trackers for good vertex resolution and the barrel Si trackers (as well as micromegas and TOF) for recoil proton detection in $\vec{A}(\vec{e}, e'p)$ to determine the product of beam and target polarization, $P_b P_t$ (see below). Finally, we will need the same Møller beam polarimeter, raster magnets, and other beam devices as the approved structure function program on polarized proton and deuteron targets. As outlined above, we plan to use two target cells, each 2 cm long and 2 cm in diameter, separated by 2.8 cm, together with about 15 nA of polarized beam, for a total luminosity of 2×10^{35} e^-/s $\times$ nucleons/cm^2 (or 1×10^{35} e^-/s $\times$ protons/cm^2, which is the nominal luminosity that CLAS12 is expected to operate under). This number includes all foils, coolants etc. traversed by the beam. The beam current and position will be monitored with the standard beam devices, including the Faraday cup.

For the following estimates, we assume a beam polarization of 0.85 (which has become standard in recent experiments at Jefferson Lab), and a target polarization of 0.8 for ^{7}Li and 0.85 for H (see above). We also assume 50 days (at 100% efficiency) of data taking, all at 11 GeV beam energy. We will trigger the DAQ on single electrons, using the highly selective combination of high threshold Cherenkov counter (HTCC) and a signal above threshold in the calorimeter (the standard CLAS12 trigger). If necessary, further reductions in rate can be achieved by matching the triggering sector of each of these detectors with a high-momentum track in the drift chambers (DC). We expect an overall event rate around 10 kHz. We have embarked on a detailed simulation of all aspects of the experiment, using the standard CLAS12 simulation package "GEMC" combined with a PYTHIA-based event generator and the tracking and reconstruction software under development for CLAS12 (with significant contributions from UTFSM). Because this software is still in preliminary form, some of the physics results presented below are obtained with the event generator described in Section I D and a simpler parametrization of CLAS12 resolution and acceptance, FASTMC.

1. Background Simulation

Beam-induced background (from electromagnetic processes) has been studied in detail for CLAS12. As an example, Fig. 14 shows the implementation of the CLAS12 region 1, 2 and 3 drift chambers in GEMC, and the assumptions (consistent with the present proposal) leading to occupancies of $0.5 - 1.2\%$ in these drift chambers. Past studies of reconstruction efficiencies have shown that at these background levels, they are reduced by a moderate amount that is not strongly luminosity-dependent.

While the proposed experiment is not significantly different from the arrangement studied in Fig.. 14, we have implemented the new two-cell polarized target with all ancillary material into GEMC and are now repeating these studies, including the full CLAS12 detector materials. An example is shown in Fig. 15, which corresponds to 10000 incoming beam particles (or 0.1 μs). At this point, we have not found any serious issues that would invalidate the general conclusions about CLAS12 efficiencies contained in the conceptual design report.

2. Resolution

For the purpose of the proposed experiment, we have to demonstrate that the CLAS12 tracking resolution is sufficient for three related quantities:

1. The resolution in vertex position for the scattered electron (and the proton for $(e, e'p)$ coincident events) has to be sufficient, in particular in the direction of the beam (z), to separate events coming from either of the two target cells, and to minimize the contribution from liquid Helium and entrance and exit foils to the measured signal (which is diluted by these contributions).

2. The resolution in x must be good enough to avoid additional "smearing" at large x, where the structure functions are dropping rapidly.

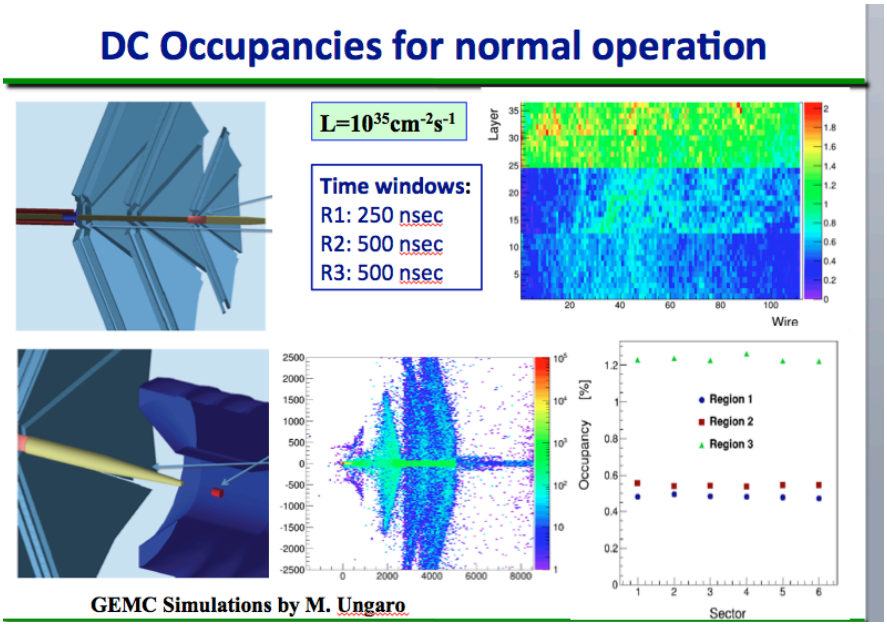

FIG. 14. Studies of beam-induced backgrounds in CLAS12 by M. Ungaro.

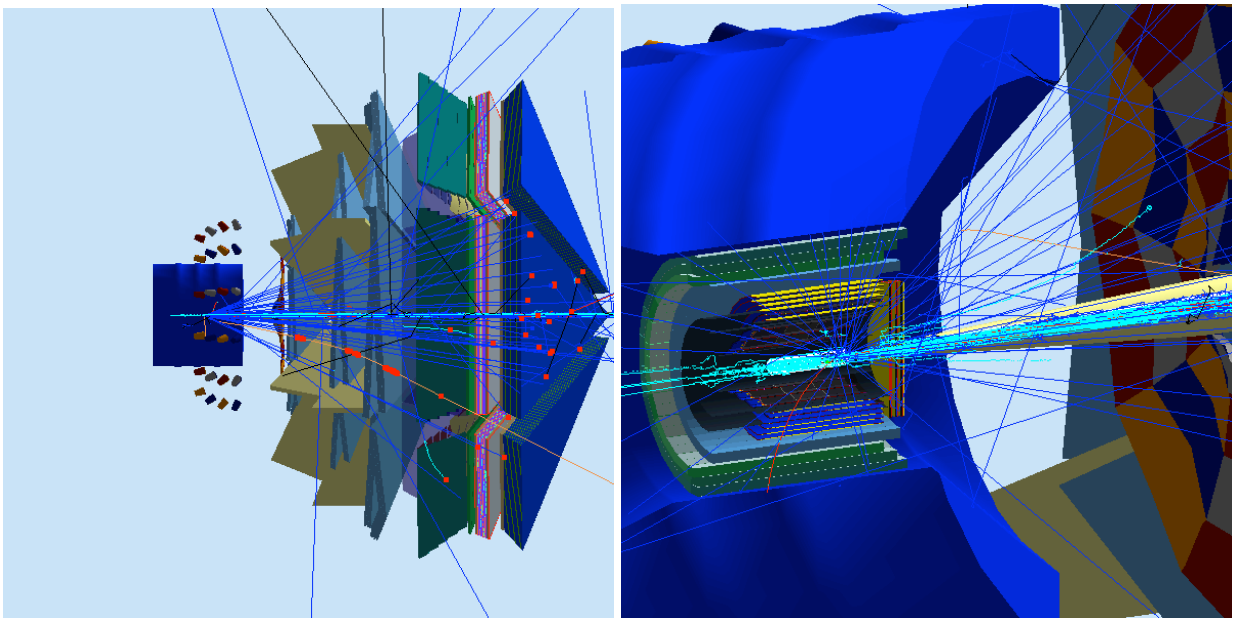

FIG. 15. First results from the implementation of the proposed polarized target into the CLAS12 simulation software.

3. For the determination of the product of beam and target polarization, $P_b P_t$ (see below), we need to have sufficient resolution to measure missing momenta and missing energies in the $(e, e'p)$ reaction to better than 0.1 GeV/c or 0.2 GeV.

We have embarked on a detailed simulation of the complete experimental set up, including the polarized target, using the standard CLAS12 simulation package GEMC, a PYTHIA-based event generator and the CLAS12 reconstruction software. Figure 16 shows a typical simulated event and a comparison of thrown and reconstructed track hits. We note that at the time of this writing, the CLAS12 reconstruction software is not yet quite complete, so that the results shown in the following are based on FASTMC instead. We expect to have up-to-date results later this year.

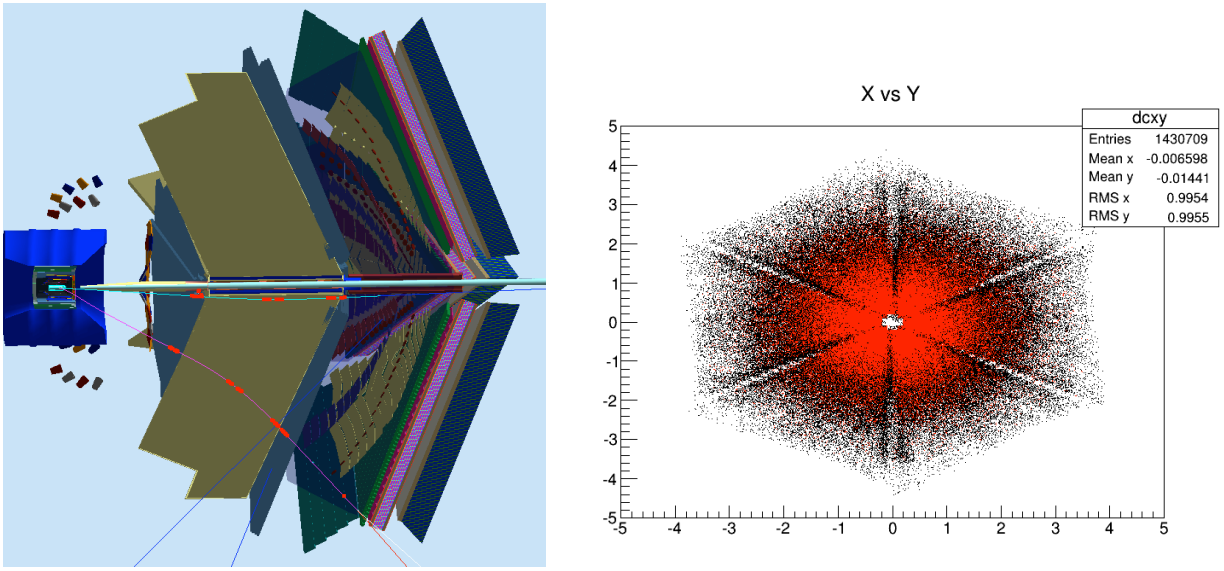

FIG. 16. LEFT: A typical simulated result within CLAS12, based on a full implementation of the proposed experimental set up. RIGHT: Comparison of generated (black dots) and reconstructed (red dots) track positions for a few thousand events

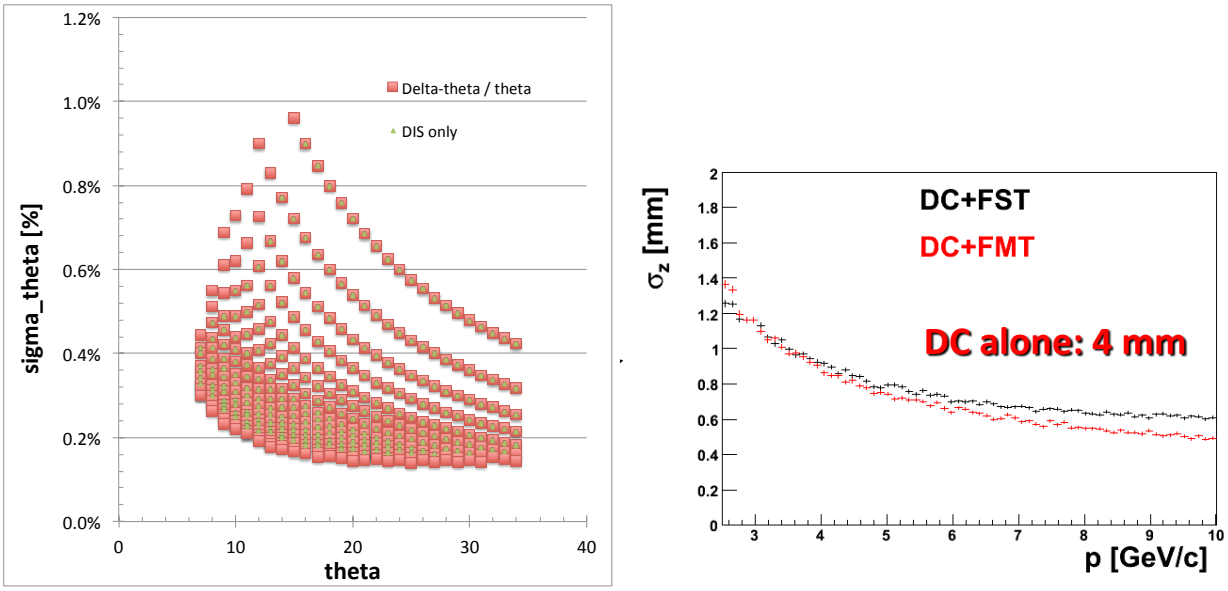

FIG. 17. LEFT: Angular resolution from FASTMC. RIGHT: Prediction for the vertex z resolution, including forward vertex tracker (simulation done by Sebastién Procureur).

For quantitative estimates of the various resolutions listed above, we use the FASTMC code which underlies the technical design report for CLAS12 and which has been validated against earlier versions of the CLAS12 tracking software. FASTMC contains both a parametrization of the CLAS12 acceptance (see next subsection) and the resolution of the forward drift chambers, assuming time-based tracking. As an example, we show in Fig. 17 the resolution in the polar scattering angle versus its magnitude. The different points at each θ belong to different kinematic points in the (x, Q^2) plane and cover all of the kinematics of the proposed experiment. As can be seen, the angular resolution is always better than 0.1 degrees (1%) in all cases. This would translate into a z-vertex resolution of better than 0.3 cm if one ignores the uncertainty in the x and y values of the vertex. The latter could be determined to sub-mm precision using the forward vertex tracker (micromega) detector that will be part of CLAS12, leading to a z vertex resolution at the 1 mm level. This agrees well with a study done with a previous implementation of CLAS12 tracking

by S. Procureur, see Fig. 17, which assumed an "infinitely well-known" beam axis.

For a more realistic estimate of the z resolution, one has to include the uncertainty on the position of the beam transverse to the z-axis. This becomes in fact the leading contribution to the overall z resolution, especially for polarized target experiments, where the beam must be rastered over the full 2 cm diameter cross section of the target material to avoid local depolarization. We will use a fast readout of the raster magnet currents at the moment of each event to calculate this beam position; the calibration of x_{Beam} and y_{Beam} as a function of these current ADC readouts will be performed on the full data set, using events with two coincident particles in the final state. By tracing back both particles to their distance of closest approach, one can determine the vertex with $\approx$ 1mm precision per event, and by averaging over many such events, the calibration constants can be determined with high precision. Still, both the short time lag involved in the readout and other uncertainties will lead to an overall uncertainty of about 1 mm of the transverse position of the beam, which translates into up to 1 cm uncertainty in the z vertex position in the worst case (forward scattering angle). Combining both the transverse uncertainty and the angular resolution, we arrive at the overall z vertex resolution (RMS) shown in Fig. 18.

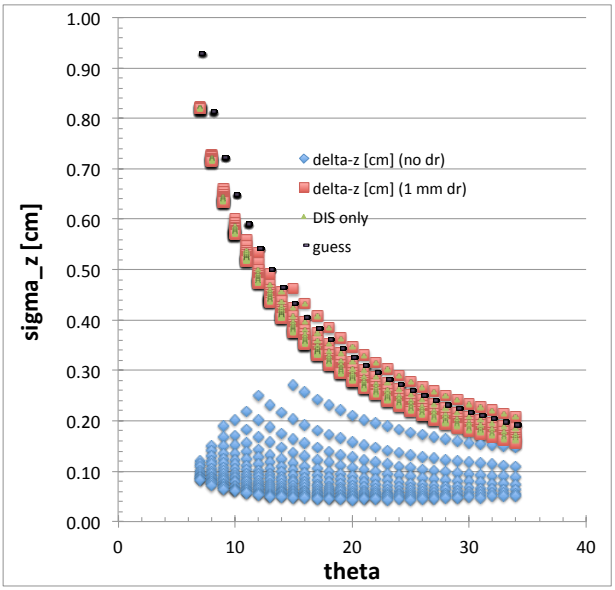

FIG. 18. Final result for the resolution in z vertex, as a function of scattering angle. Different points belong to different kinematics at the same scattering angle..

As can be seen, the resolution is always better than 1 cm, and becomes progressively better at larger scattering angles. By using an optimized cut on the reconstructed z-vertex (roughly 1 standard deviation beyond the physical length of each target cell), we can optimize the overall figure of merit by minimizing the loss of events from polarized material that fall outside the cut versus the dilution through unpolarized liquid Helium coolant which contributes to events inside those cuts. Because of the 2.8 cm separation between the two cells, cross talk (events from one cell being assigned to the other) is minuscule (less than 1%). The same is true for the exit and entrance foils of the liquid Helium containment vessel, and all heat shields and other target windows.

Finally, in Fig. 19 we show the resolution in the kinematic variables x and W, again according to FASTMC simulations covering the full kinematic range of the experiment. The resolution in x is always better than 2% (including both momentum and angle resolution), which means that our highest x bin (around 0.775) will have an intrinsic width of less than 0.016. By averaging over bins of size 0.05, the intrinsic x resolution plays only a very minor role and can be modeled accurately in our Monte Carlo predictions for the experiment.

The resolution in W is better than 60 MeV above the limit of the resonance region (solid vertical line), while it becomes significantly worse below that. For elastic scattering ($W = 0.94$ GeV), the 1-sigma width is about 140 MeV, which corresponds to the required resolution in missing energy quoted above. Therefore, overall we conclude that the expected resolution of CLAS12 in all relevant kinematic variables will be adequate for the proposed experiment.

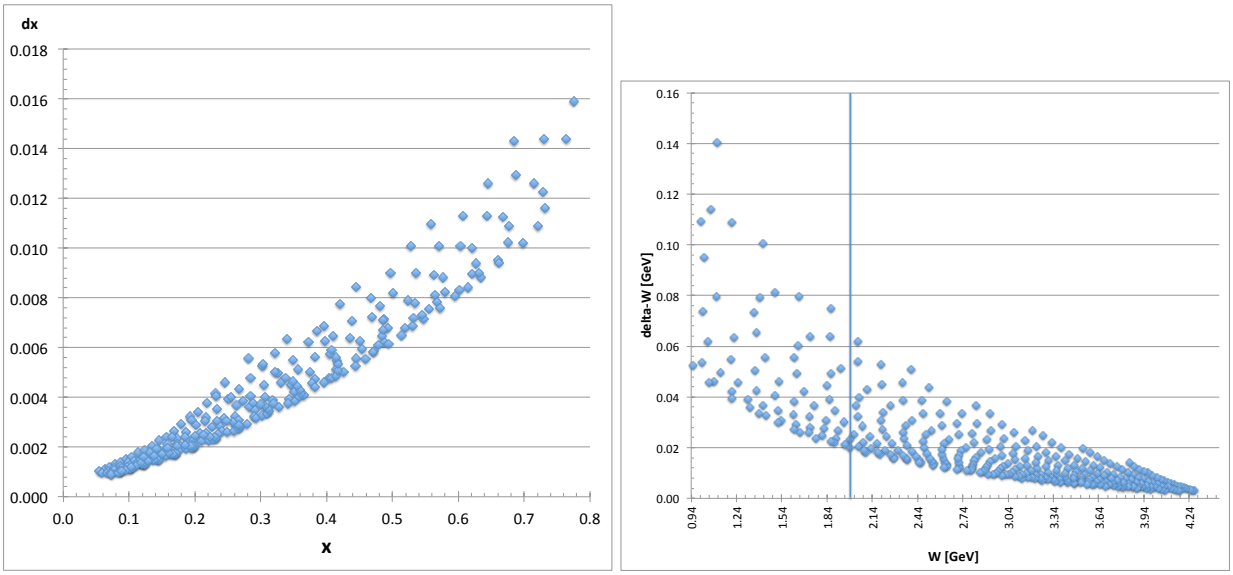

FIG. 19. LEFT: Resolution in the Bjorken x variable from FASTMC. RIGHT: Resolution in final state mass W.

3. *Acceptance*

The same FASTMC simulation, together with a more sophisticated model for spin structure functions including nuclear effects (described in Section I D) was also used to determine the expected rates in all kinematic bins. The acceptance of CLAS12 is modeled separately for both the forward tracker (three layers of DC, Cherenkov counters and calorimeter) and the central detector, including a realistic implementation of the magnetic fields from both the torus and the central solenoid. For our predicted statistical uncertainties, we use the predicted rates from all target components, including unpolarized species like liquid Helium coolant or lightly polarized species like the deuteron and ^{6}Li, carefully including the effects of our proposed z vertex cut (see above). For the main (inclusive) measurement, only electrons detected in the forward tracker are counted, while for (quasi-)elastic $(e, e'p)$ events, we take into account events where the proton is either detected in the central detector or in the forward tracker (the latter is much less probable). The complete kinematic coverage of the experiment can be read off Figs. (10,19). We will discuss the resulting statistical and systematic error estimates in the next two sections.

C. Expected Results

1. *Inclusive Results*

In the following, we discuss the expected results from the proposed experiment for the two ratios R_1 (Eq. 26) and R_2 (Eq. 28) defined in Section I C. We use the generator described in Section I D 2 (with some $x-$rescaling due to the treatment of off-shell effects) and FASTMC to calculate the number of events in each of 15 bins in x and up to 4 bins in Q^2. We apply a cut to only count events in the DIS region, $Q^2 > 1$ GeV^2 and $W > 2$ GeV. We also simulate the background from deuterons (in the case of ^{7}LiD), ^{6}Li for the proton target, and the Helium coolant, within the vertex cuts we will apply (with full consideration of smearing effects). We compare the results, together with their expected *statistical* errors, to several of the models described in Section I D in Fig. 20 and Fig. 21.

Figure 20 shows the ratio R_1 which is essentially equal to the ratio $g_{1^7\mathrm{Li}}(x, Q^2)/g_{1p}(x, Q^2)$ but can be determined directly from the data as the ratio of the cross section *difference* for the two beam helicities on ^{7}Li over that of the proton. We show the results for 4 different (large) bins in Q^2 (slightly offset for better visibility) which could either be combined for even better statistical precision or compared to Q^2-dependent models (which do not exist yet but could be obtained within several of the model frameworks described earlier, e.g. by applying DGLAP evolution). We note several salient observations in Fig. 20:

- While the naïve nuclear model (NMM) and the standard nuclear model (SNM) are very close to each other at low x, they differ in the mid-to-high x range by up to 5% (which is an indication for the uncertainty due to nuclear

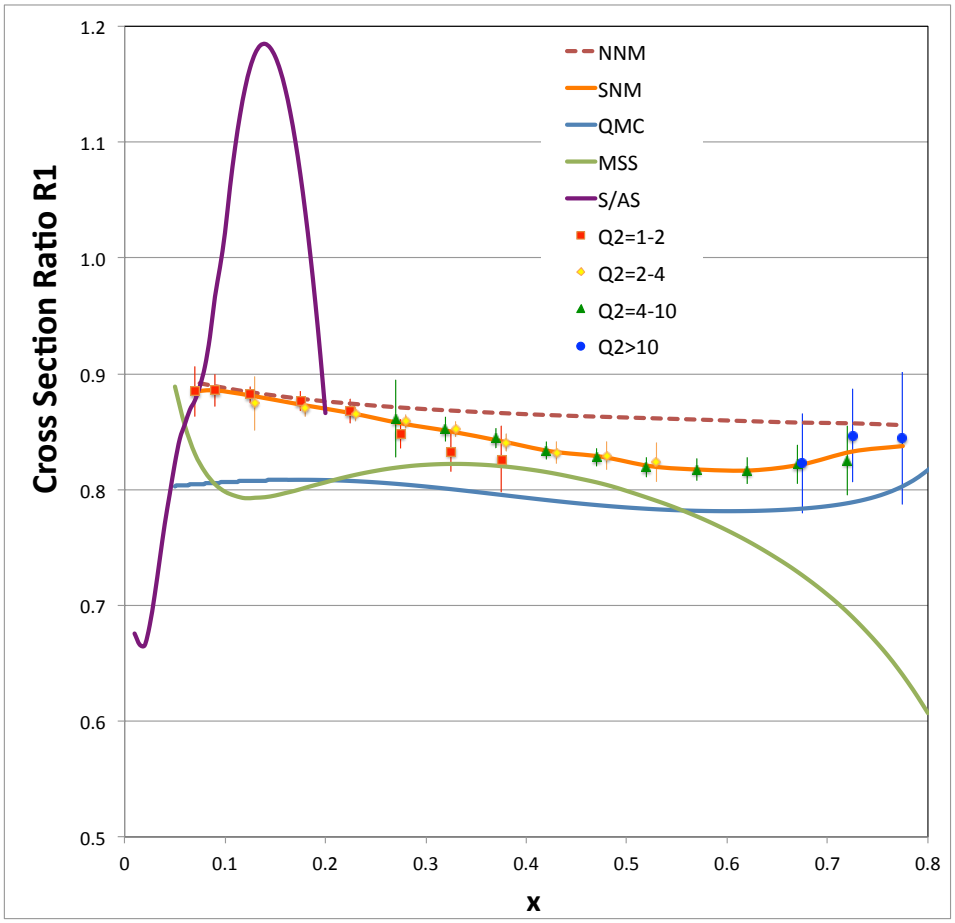

FIG. 20. Ratio R_1 of cross section differences for $^7\vec{\mathrm{L}}i(\vec{e},e')$ over $\vec{p}(\vec{e},e')$ for several different models (NNM = naïve nuclear model, SNM = standard nuclear model, QMC = Quark-meson coupling model, MSS = modified sea scheme, S/AS = shadowing/antishadowing model). The expected data for several different Q^2 bins are shown together with their statistical error bars.

effects outside the EMC effect). Clearly, we will be able to distinguish even between these two "nucleons-only" models with good statistically significance.

- In the "mid-x" range $0.2 \leq x \leq 0.6$, the two models shown that include a strong genuine EMC effect are significantly belwo the "nucleon only" curves, although all models apart from the NNM are similar in that range. Beyond $x = 0.6$, there seems to be strong divergence between the MSS model and the QMC model; however, the former does not contain any treatment of Fermi motion effects, which would make this difference less pronounced.

- It is clear that in the region $x < 0.2$, the various models show strikingly different behavior, easily distinguished within the precision of the proposed data. All models with genuine EMC effect are significantly separated from the NNM and SNM expectations (which are nearly identical in that region); however, they differ even in the *direction* of that deviation (up or down). The purple curve (the shadowing/anti-shadowing model by Guzey and Strikman) could of course take a somewhat different shape, but even if the enhancement around $x = 0.15$ were only 1/3 as large, it should be easy to ascertain its existence (or otherwise). The Chiral Quark Soliton model (not shown) would probably fall somewhere between the green and the purple curve, again separated from all others by several statistical standard deviations.

In summary, it is clear that the proposed experiment will have enough statistical power to easily detect an EMC-like effect in the spin structure function g_1 in ^{7}Li, and study its $x-$ and Q^2 dependence in considerable detail. The question remains whether such an EMC effect might turn out to be simply due the well-known unpolarized EMC

effect, which could affect F_2 and g_1 by the same factor. This is clearly *not* the case for most of the models we have studied so far, as Fig. 21 shows.

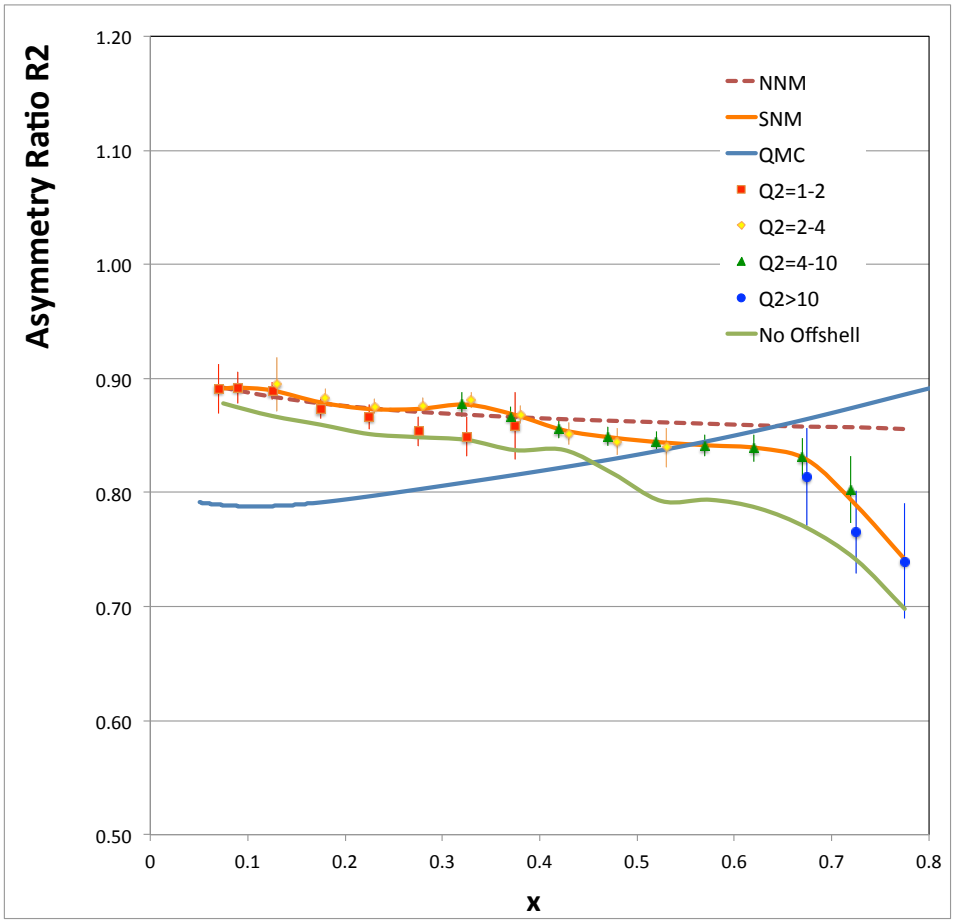

FIG. 21. Ratio R_2 of the parallel double spin asymmetry $A_{||}$ for $^7\vec{\mathrm{L}}i(\vec{e},e')$ over $\vec{p}(\vec{e},e')$, normalized by multiplying it with the "naïve " unpolarized structure function ratio for ^{7}Li over hydrogen. Some of the same models as in Fig. 20 are shown, together with the data and their statistical errors.

In this figure, we display the ratio R_2 of the inclusive double spin asymmetries $A_{||}$ on ^{7}Li over the proton, normalized by the naive cross section ratio for 7 nucleons over 1 proton (see Section I C). This ratio is a close representation of the EMC effect in the polarization asymmetry A_1, which is largely independent of the **un**polarized EMC effect. As for R_1, absent *any* nuclear effects, this ratio would be unity. The dashed line shows the expectation from taking into account the effective polarization of proton and neutron in ^{7}Li only. The standard nuclear model (SNM) leads to a significant change of this expectation only at high x.

Not accounting for any nuclear binding at all, Fermi smearing alone will lead to an overall reduction of the asymmetry (green "No Offshell" curve). While Fermi smearing plays little role in the usual (unpolarized) EMC effect up to fairly high x, due to the fact that the structure function F_2 has only a mild $x-$dependence in that region, the asymmetry A_1 (or $A_{||}$) is a monotonically rising function of x, which makes Fermi-smearing important over the whole range. Interestingly, adding off-shell effects (which is similar to assuming x-rescaling) to the picture (orange curve) largely compensates for this effect, since larger x translates into larger asymmetry. On the other hand, the QMC model (blue curve) shows a nearly opposite effect in the asymmetry – while the modification of spin structure functions in this model is a lot stronger than for the unpolarized structure functions in general (leading to the strong suppression at small x), this is not true at larger x where the suppression is pretty much the same for both numerator and denominator entering the asymmetry. Finally, adding any kind of sea quark enhancement (as proposed by the CQS, shadowing/anti-shadowing or the MSS model) would lead to a big enhancement of the asymmetry at low x. Again, it is clear that apart from the overall scale of the reduction, the precise $x-$dependence of the ratio R_2 differs strongly between models, significantly more than the statistical errors of the proposed experiment.

2. (Quasi-)elastic coincidences

In addition to the inclusive asymmetries and cross section difference ratios, we will also measure elastic $\vec{p}(\vec{e},e'p)$ on the proton target and the same reaction in quasi-elastic kinematics on the ^{7}Li target. In both cases, the cross sections are largest for relatively low $Q^2 \approx 1.2 - 2.4$ GeV, where the electron is scattered at small angles into the forward tracker while the proton is detected in the central detector at moderate momentum (1-2 GeV/c). While the corresponding asymmetries are rather small, they can be measured with very high precision and directly related to the product of beam and target polarization in both cases. This has been used as the standard method to determine this product for all of the recent spin structure function experiments in Hall B.

In the case of the free proton, the double spin asymmetry is well known, with high precision, from measurements in the 6 GeV era of Jefferson Lab. It can be written exactly like the corresponding inelastic asymmetry $A_{||}$, see Eq. 6. Here, it is important to note that the by far dominant term is due to A_1 which for elastic electron-proton scattering is equal to 1 by definition. The correction due to $A_2 = \gamma G_E/G_M$ is relatively small for target spin parallel to the beam, and it turns out (fortuitously) that the dependence on the ratio G_E/G_M is further diminished by the factor $1 + \epsilon R$ in the denominator of $A_{||}$, where $R = A_2^2$, which partially compensates for the contribution from A_2.

For the same reason, $A_{||}$ is not expected to be significantly modified by any nuclear effect. While there exist measurements of the ratio G_E/G_M in ^{4}He that have been interpreted as a slight change in this ratio [57], these measurements used the *transverse* polarization component of the outgoing proton, which is much more sensitive to this ratio. We can safely assume that the model uncertainty due to G_E/G_M (which could be even partially corrected for using the results from [57]) is below 1% for both the proton and for ^{7}Li.

For the proton, the dominant uncertainties in extracting $P_b P_t$ are the statistical uncertainty and the dilution by other target material. The latter is very well under control since the reconstruction of all final state particles allows one to apply very tight cuts on missing momenta, which will all but eliminate the contribution from target materials like ^{6}Li and liquid helium. Experience with experiments EG1 and EG1-dvcs show that one can reduce these contributions to less than 10%, with a sub-% uncertainty. Finally, we used the same simulation described above to estimate the statistical uncertainty, which turned out to be 0.5% after averaging over all accepted Q^2 bins. Therefore, we conclude that we can measure the product of beam and target polarization with an absolute uncertainty of 1% for the proton target. Given similar precision from the Möller measurement of beam polarization, we can use this result also to calibrate the independent NMR measurement of the proton polarization (to maybe 2-3%).

For the case of ^{7}Li, the case is of course more complicated. Our simulation shows that we can achieve a statistical accuracy of 1.2%, which is partially explained by the fact that only one of three protons carry polarization. On the other hand, the dilution by other target materials (D and liquid Helium) will be more substantial (about 40% of all events will come from these). The reason is of course that we cannot use very tight cuts on missing momenta, since the polarized proton inside ^{7}Li is in a p-wave which has substantial strength out to momenta of about 300 MeV/c. We will use a cut around that value (or somewhat below, to optimize the figure of merit) which is included in the uncertainty quoted above. To determine the dilution factor accurately, we will need to measure the rate from the same target set up with all solid target material removed. Again, experience with previous experiments shows that we should be able to achieve a precision of maybe 2-3% on the dilution factor, which will be the dominant error in the case of ^{7}Li.

We will once again use a complete standard nuclear model, including momentum distributions and effective polarization of the proton, to calculate the theoretical expectation for the measured asymmetry in ^{7}Li. This model should be able to predict the asymmetry as a function not only of Q^2 but also of the missing momentum and its direction. (This can be used to validate the model). Finally, it should include final state interactions (FSI) between the outgoing proton and the nuclear remnant. This is certainly challenging, but not unachievable. Recently, Jeschonnek and van Orden [58] developed a complete calculation for the case of the deuteron, including a realistic FSI with spin degrees of freedom for the outgoing nucleons. The underlying spin-dependent nucleon-nucleon scattering amplitudes have been extended [59] to the high c.m. energies necessary for 12 GeV electro-disintegration. This model was tested with measurements of the missing momentum dependence of the asymmetry $A_{||}$ using the existing deuteron data from EG1b [60] and found to give a good description, even at high missing momenta up to 500 MeV/c. Fortunately, it was also found the FSI play a minor role at lower missing momenta, where the PWIA picture alone does a very good job describing the asymmetry data. While it is clearly more difficult to apply this model to a nucleus like ^{7}Li, the basic ingredients are all in place. Furthermore, with the precision achievable, we can even test whether the effective nuclear polarization is correctly predicted by modern wave function models of ^{7}Li, since the asymmetry will be mostly sensitive to that quantity (not the overall nuclear polarization). In summary, measuring the quasi-elastic asymmetry on ^{7}Li will provide precise results of significant interest in their own right, while at the same time providing an overall cross check on the product of target polarization and effective nucleon polarization within the nucleus that directly enters comparisons between our measured ratios R_1 and R_2 and models of the polarized EMC effect.

D. Systematic Uncertainties

In this section, we discuss the impact of various systematic uncertainties on the achievable precision of the two ratios R_1 and R_2. We separately consider point-to-point systematic uncertainties (which enter the $x-$ and Q^2-dependence of these ratios) and overall scale uncertaintes that would move all data points by the same fractional amount.

1. Beam and target polarization

In both ratios, the product of beam and target polarization enters directly in both the numerator and the denominator. In particular, since both target cells will see the same beam, its polarization will cancel completely in the ratios. However, we will monitor the beam polarization using the standard CLAS12 Møller polarimeter about once a day, to be able to make an absolute prediction for the elastic double-spin asymmetry for the proton (see previous Section).

The target polarization will be measured using the standard NMR technique for solid polarized targets [61]. Both target cells will have identical (as far as possible) resonant circuits driven by Liverpool NMR cards. Both of these NMR systems will be calibrated by measuring the thermal equilibrium signal for both targets during extended beam shut down periods. Since the magnetic moment of both the proton and of ^{7}Li are well known (to better than 1%), the systematic uncertainty on these TE measurements will be dominated by the accurate measurement of the temperature (maybe a few %, but the *same* for both targets), and the magnetic field (known to better than 10^{-4}). It will be important to have sufficiently long time intervals for these measurements, to guarantee that the targets have really reached thermal equilibrium and to minimize the statistical error on the measurement of the very small signal. From experience with other (polarized proton) experiments, we believe that we can achieve a systematic error on the calibration of less than 3%. The corresponding error on the ratio of target polarizations will be even smaller, in particular since we are planning to exchange the two target materials halfway through the experiment while keeping the NMR circuits unchanged. We budget a total scale error on the two ratios of 2% as a safe upper bound.

In addition to the direct ("brute force") measurement of the ratio of target polarizations, we will also employ a completely independent check, which also addresses the question of the "effective polarization" of the proton in ^{7}Li. For this purpose we will use coincident $(e, e'p)$ events on both targets, with cuts to select either elastic events (for the proton) or quasi-elastic events (for ^{7}Li) (see previous section).

In summary, while we keep the uncertainty estimate for the two ratios due to beam and target polarization at a safe upper bound of 2%, we can check the accuracy of both NMR measurements to better than 1.5% and, in the case of ^{7}Li, determine whether the prediction of the standard nuclear model for the effective proton polarization in the nucleus is correct. Therefore, we assign a combined experimental and model uncertainty to the overall scale factor on the ratios of less than 3%.

2. Dilution by unpolarized target material and target density times acceptance

In the case of ratio R_1, the contribution from unpolarized target material does not enter at all, since it is directly a ratio of cross section differences for opposite sign of the product $P_b P_t$. However, it is affected by the slightly different acceptance of CLAS12 for the two target cells. To minimize such differences, we will use a fiducial cut that gives the same acceptance in azimuthal angle for both target cells, as well as the same coverage in Q^2 for each x bin. Remaining differences due to localized detector inefficiencies can be corrected for using the Monte Carlo simulation which we have already begun. However, in any case they will cancel out due to the interchange of the target material between the two cells that we plan for (at least) the half-way point of the experiment. Vice versa, temporary changes of acceptance due to overall tracking efficiency, Cherenkov gas composition, detector trips etc. will affect both target cells simultaneously, which means they largely cancel. We assume a point-to-point uncertainty of perhaps 2% as well as an overall scale uncertainty of 2% on the ratio R_2 due to any remaining, uncanceled acceptance effects. We note that these estimates are quite realistic in light of recent experience with CLAS; both the TPE experiment [62] and the G_{Mn} experiment [63] measured similar cross section ratios with less than 2% systematic errors. Similarly, we also need to know the ratio of total target areal density for both targets to extract the correct cross section ratio. Fortunately, lithium hydrides are chemically stable and solid even at room temperature if kept in an inert atmosphere. Therefore, we will be able to measure the total amount of target material in either cup after the measurement. Given the geometry of each cup (which we can photograph) and the raster pattern, we believe that a total scale uncertainty of 2% can be achieved. We will look at additional methods to improve this precision; for instance, the cross sections for elastic proton scattering and for deuteron quasi-elastic break-up are known with high precision, and their ratio has model uncertainties that are not too large for this purpose. (We can again minimize contributions from other

target components when measuring these cross sections by detecting both an electron and a proton in coincidence and applying tight cuts, e.g., on the missing mass).

Conversely, in the case of the ratio R_2, acceptance effects and total luminosity cancel since both the numerator and the denominator of each asymmetry is measured using the *same* target (in fact, the same events), and since the beam spin will be reversed rapidly (at least 30 times a second). On the other hand, dilution due to unpolarized material is more significant, especially in the inclusive case (the $(e, e'p)$ case is discussed in the previous Section). For the free proton target, the dilution factor will be between 0.12 and 0.14, depending on kinematics. (This includes the dilution due to ^{6}Li; its polarization is treated further below). On the other hand, the dilution factor for the ^{7}Li target is much more favorable, between 0.64 and 0.70, since only the deuteron and the liquid helium coolant contribute. (Note that we do **not** include in this dilution factor the "nuclear dilution" of the polarized proton inside ^{7}Li - this is accounted for in the much lower value of the expected asymmetry on the nucleus). In either case, the dilution factor has to be determined by a combination of auxiliary measurements (in particular, a run with empty target cells and only liquid helium in place, as well as a continuous monitoring of the rates from all foils, for which we will know the exact thickness) and model calculations. In particular, we will use state-of-the-art models and parametrizations of nuclear structure functions and cross sections to predict the contribution from each component contributing to the count rate, which we can then check using these auxiliary measurements. This approach has worked very well in past polarized CLAS experiments [64]. The main uncertainties will be the packing fraction (the fraction of the target volume actually occupied by lithium hydride beads) and the effect of the vertex cuts described in Section II B. Note that both of these affect only the relatively small contribution from liquid helium (and foils), since the ratio of events from both atoms within the lithium hydrides is unchanged. This contribution is of order 20% to the total count rate, and therefore even a 10% uncertainty on its magnitude would lead to a net uncertainty of only 2% on the dilution factor. Overall, we estimate a 3% scale uncertainty due to the combined effect of all quantities entering the calculation of the dilution factor, and a 1-2% point to point uncertainty (since the dilution factor depends somewhat on x, with some model uncertainty).

3. Contribution from the deuteron and Lithium-6

To extract only the ratios of the wanted species (protons and ^{7}Li), we need to first subtract the contributions to the cross section *differences* from their polarized deuteron and ^{6}Li partners. For this, we need to know their relative polarization (e.g., $P_z(D)/P_z(^7\mathrm{Li})$) and their asymmetries and cross sections.

In the case of the ^{7}LiD target, we find that, accounting for the polarization of the deuteron (0.36 according to EST), the contribution from the deuteron can be anywhere between 15% (at the smallest x) to 50% (at the highest x) of the pure ^{7}Li asymmetry or cross section difference. Fortunately, the deuteron spin structure function g_1 and therefore the cross section difference will be measured with few % precision by the 12 GeV polarized nucleon structure function experiment. Therefore, the main uncertainty will come from the deuteron polarization. Because the same target cells will be used for both the proton and the deuteron part of the approved experiment, we will design them with NMR coils suitable for both species. This will allow us to measure the deuteron polarization directly and confirm the EST prediction. (Note that, according to Fig. 13, the EST hypothesis seems to be accurate to 1% absolute and therefore 3% relative at this particular value of deuteron polarization). We assume a safe upper limit of 5% relative on the deuteron polarization. This would yield an $x-$dependent, point-to-point systematic uncertainty of 0.4 - 2.5% to the measurement on ^{7}Li.

In the case of the ^{6}LiH target, the relative polarization is even lower, 0.24 vs. 0.85 for the proton. Since ^{6}Li can be described as a α-deuteron cluster, with an "effective deuteron polarization" of about 94% [53], the contribution to the measured cross section difference (and asymmetry) is only 10 - 30% (from lowest to highest x). Again, precise nuclear calculations for ^{6}Li exist, and the spin structure function is essentially that of a deuteron multiplied with the "effective polarization". Thus, if this effective polarization can be determined to better than 3%, we can keep the additional systematic uncertainty due to ^{6}Li below 1% at all x. The effective polarization can be measured similarly as for ^{7}Li, using quasi-elastic scattering $^6\mathrm{Li}(e, e'p)$. Because of the very sharp proton peak (that can be cut out of the missing momentum spectrum), the contribution from ^{6}Li alone can be easily isolated, and a similarly good statistical precision (1.2%) as for ^{7}Li achieved. The same arguments apply, so that we believe that the above-mentioned 3% overall uncertainty is well within reach. Again, we can compare with the prediction from EST which also should be good to within 3%, but for the ^{6}Li nuclear polarization instead.

Of course, it is possible (even likely) that there is a polarized EMC effect in ^{6}Li, as well, which would further modify its contribution to the proton measurement. However, it would seem very unlikely that this effect would be much different between ^{6}Li and ^{7}Li. So, for example, if there really is an enhancement of the ratio by 20% around $x = 0.15$ for both Li isotopes, then the extracted proton cross section difference would be in error by 2.4% at the same x, which would reduce the *measured* ratio R_1 by 2.4%, i.e. from a 20% enhancement to only a 17.6% enhancement. Vice

versa, a 10% EMC effect in ^{7}Li at high x could be reduced to maybe 7% due to the corresponding effect in ^{6}Li. Thus, while we may underestimate the total magnitude of any EMC effect, under no scenario would the deviation from the standard nuclear model "disappear" (or even largely disappear) due to the same effect occurring in ^{6}Li. Of course, one could even correct for this "dilution" of any EMC effect in both ^{7}Li and ^{6}Li.

We will continue to study ways to minimize this systematic uncertainty. Of course, we could also use standard ammonia (NH_3) for the reference target, which would all but eliminate this particular uncertainty. (Nitrogen carries very little polarization, and even less of it is carried by the individual nucleons. Combined with the more advantageous ratio of 3 H per N, the corrections are of order 1-2% in our experience, with negligible uncertainty).

Combining all uncertainties due to polarized species other than the ones of interest, we find a (largely point-to-point) systematic uncertainty of 0.5% at small x up to 2.7% at the highest x on both ratios. These uncertainties may be slightly increased if we consider the possible contribution of unwanted isotopes in each of the target materials we chose (maybe 5% ^{7}Li in the ^{6}LiH target, etc.). Based on experience with past polarized target experiments, we believe that these effects will be significantly smaller than the ones discussed above. We thus use an estimate of 1% uncertainty at the smallest x, increasing linearly to maximally 3% for our highest x point.

4. Model dependence

We have already discussed in great detail the effect from various nuclear models on the conclusions one can draw from measurements of R_1 and R_2. Here, we only mention that for the comparison to any model of these ratios, at some level uncertainties in the normal polarized and unpolarized nucleon structure functions will enter. Most of those have a small effect, which partially cancels in the ratios. We did a detailed study of the contribution coming from the correction due to A_2, i.e. the expressions $C_p(A_2)$ and $C_{^7\mathrm{Li}}(A_2)$ in Eqs. 26,28. As an extreme case, we replaced our standard parametrization of the world data on A_2 by simply setting A_2 to zero everywhere. Since these corrections appear both in the numerator and the denominator of the ratios, the effect is minimal - we found a change of much less than 1%. Other structure function inputs have similar effects. Therefore, we estimate an upper bound of 1% (point-to-point) for all of these uncertainties combined.

5. Radiative corrections

Both the asymmetries and the cross section differences for either target (^{7}Li and H) will be corrected for e.m. radiative effects, including the energy (and polarization) loss of the incoming and outgoing electrons in the material of the target. For the latter (external) corrections, we will use the full implementation of our set up in GEMC, which is based on GEANT4 and contains all the relevant physics. We will cross-check the results using the prescription by Mo and Tsai [65] using the target thickness in radiation lengths. From past experience, we expect an uncertainty on these effects at the % level, which is further reduced by the fact that we measure ratios from two targets and that we will exchange the sequence of these two targets. We will apply a cut on the maximum energy loss ν to avoid regions where radiative effects (as well as pair-symmetric electron production) become too large for the necessary precision.

The internal radiative corrections will be based on the formalism by Kukhto and Shumeiko [66] and the application of that formalism for nuclear targets [67]. We will work with the first author of [67] to implement this formalism and put a firm upper bound on the resulting uncertainty. We emphasize that several of the authors on this proposal have extensive experience with the development of radiative correction code for both polarized experiments (EG1, EG4) and for nuclear targets (EG2). Our experience convinces us that we can reach a total systematic error on all radiative corrections of less than 2% point-to-point.

6. Summary of systematic uncertainties

In summary, we find (by adding all systematic uncertainties listed above in quadrature) that the overall systematic uncertainty on each of the two ratios is roughly equal. The point-to-point uncertainty ranges from 3.2% at low x to 4.2% at high x, while the overall scale uncertainty is 4%. We note that the uncertainties on the two ratios are partially independent, since different effects contribute. We list the main sources of systematic uncertainties in Table I.

In Fig. 22 we show again our expected results, this time with systematic point-to-point uncertainties added in quadrature to the statistical ones. Once again, we conclude that our data will have sufficient precision to distinguish between the rather different $x-$dependence predicted by various models. While scale uncertainties could move all data points up or down by up to 4%, this would not affect the $x-$dependence and is still small enough to measure an overall depletion of the in-medium spin structure function below the naïve nuclear model in excess of 5%. Clearly,

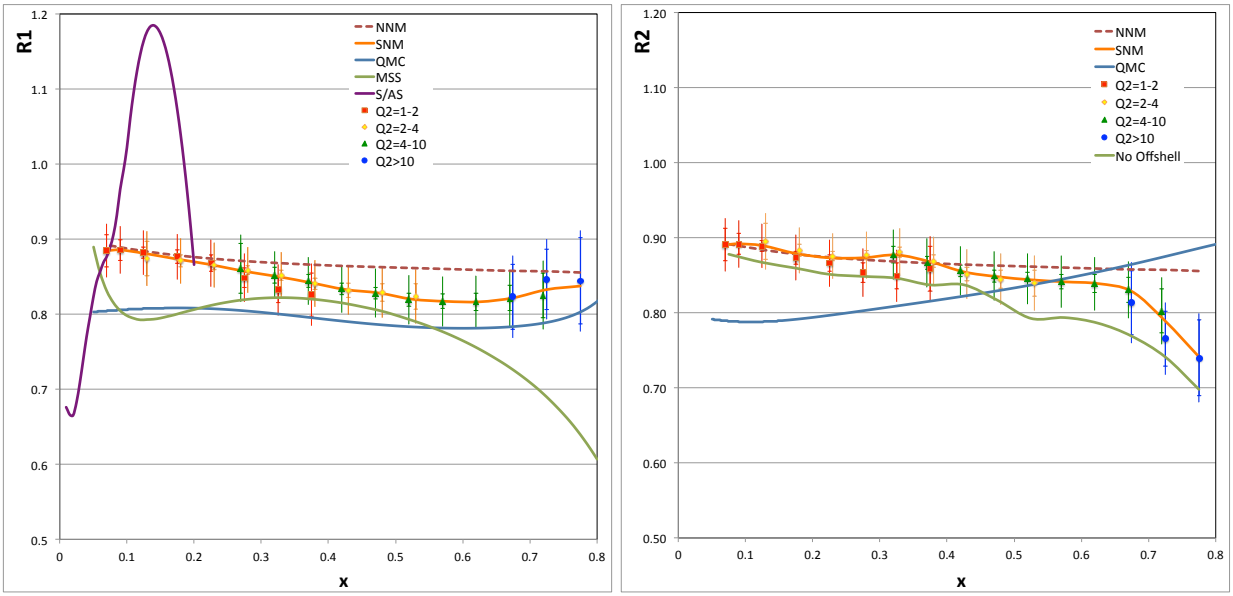

FIG. 22. Expected results for both ratios as in Figs. 20 and 21, with point-to-point systematic uncertainties added in quadrature (total length of error bars) to the statistical ones (horizontal bars). An overall scale uncertainty of about 4% is not shown

TABLE I. Expected point-to-point systematic uncertainties by source. An overall scale uncertainty of about 4% is not included. Where a range of values is given, it refers to the magnitude of the systematic uncertainty at low *vs.* high x.

Source	Rel. unc. on R_1	Rel. unc. on R_2
Dilution	2%	–
Acceptance	–	2%
Polarized background	1% – 3%	1% – 3%
Model uncertainties	1%	1%
Radiative corrections	2%	2%
Total	3.2% – 4%	3.2% – 4%

our measurement will be most sensitive to EMC effects at low to moderate x, including any significant enhancement at $x < 0.2$ as predicted by several models or the significant depletion within the QMC model. Vice versa, at the high-x end, there are also significant differences between the models which should allow us to find the best-matching one with a significant difference in χ^2 for our anticipated data. Because of the very high importance of the low- and high x limits, we have budgeted the amount of requested beam time to ensure that statistical errors are smaller or at most comparable to systematic ones in these regions.

III. BEAMTIME REQUEST

We request 50 days (1200 hours) of "100% efficient" beam time, with 15 nA highly polarized (> 0.85), 11 GeV electron beam on target in Hall B. Assuming close to 80% polarization for the ^{7}Li target, the collected number of events with this amount of beam time will suffice to keep the statistical errors comparable to or smaller than the systematic ones in the important low-x and high-x regions (except for the highest Q^2 points where statistical errors will dominate). With these optimistic (but not unrealistic) assumptions for target and beam performance, 50 days will suffice to maximize the discovery potential of the proposed experiment.

We request an additional 5 days of beam time for necessary target maintenance operations, such as additional cold irradiation, TE measurements, anneals, target (re-)polarization, exchange or replacement of target material, and including at least one day of running of pure liquid ^{4}He for dilution factor studies. We expect the time required for commissioning of the experiment *with beam* to be minimal, assuming it can be scheduled shortly after the approved

run for longitudinally polarized proton and deuteron targets [51].

All necessary calibrations can be done either before the experiment (without beam in the Hall) or during extended shut down periods, or in parallel with normal data taking. In particular, some time of order 1-2 weeks without beam will be needed both before and after the run, to optimize the target performance *in situ* and to measure the thermal equilibrium (TE) signal. Installation and de-installation of the longitudinally polarized target in CLAS12 will take roughly an additional week or two; again, this overhead would be minimized by running both the nucleon and the nuclear program in sequence.

IV. SUMMARY

After nearly 40 years, the fundamental mechanisms underlying the EMC-effect (the modification of nucleon structure functions in nuclei) have yet to be completely clarified, within a QCD-based description that is generally accepted by the community. Such a solution of the "first EMC puzzle" is a necessary step towards a full understanding of QCD in the strong binding regime, including properties like confinement and nuclear structure. Jefferson Lab at 12 GeV is probably the last, best place to bring the most complete and precise data set to bear on this problem, from inclusive as well as semi-inclusive measurements, on a wide range of nuclei. Polarized structure function have an important role in this program, since they might well be affected in a significantly different way than unpolarized ones (according to several models we describe in this proposal). Any program to map out all aspects of the EMC effect would remain incomplete without the proposed data. (Spin effects have more than once proven to be the decisive factor in rejecting or modifying theoretical assumptions that seemed to describe unpolarized data well enough - see the "second EMC puzzle" as an example).

We have attempted to demonstrate that with 50 days of new beam time on a polarized ^{7}Li target, we can decisively test (and possibly reject) various predictions for the polarized EMC effect, most of which differ both in magnitude and in their $x-$dependence from each other and from the highly precise "standard nuclear physics" calculations that are now available. Statistical and systematic uncertainties are under control and will be small enough for a highly significant measurement. We believe that the proposed experiment would be one of the corner stones of the program to rigorously examine the EMC effect and its causes at Jefferson Lab with 12 GeV.

V. OUTLOOK

The present experiment is the first step in a thorough exploration on the modification of polarization-dependent parton distribution functions in the nucleus. We expect that additional proposals will make use of the same beam time (if approved) to measure, for instance, semi-inclusive or deep exclusive single target and double beam-target spin asymmetries on a proton embedded in the nuclear medium. The topics addressed range from a more detailed picture of quark propagation and hadronization to a better elucidation of the final state interaction that plays a big role in some TMDs. Accordingly, several letters of intent are either under development or will be submitted to the PAC concurrently with the present experiment. Typically, these additional experiments will require detection and identification of leading hadrons (pions and kaons) in the forward direction, in addition to the scattered electron.

Beyond these measurements on ^{7}Li, it is conceivable that the results are compelling enough to require further measurements on other nuclei, both to confirm any observed effect and to study its systematic dependence on A. We have looked at several possibilities, including ^{11}B and ^{19}F, two nuclei where a single proton carries most of the nuclear spin. While there aren't truly microscopic calculations available yet for the heavier of these two, it is quite clear that ^{19}F may be an intriguing candidate, since the valence proton is in the $2s_{1/2}$ shell, which makes this a particularly "proton-like" target. Recent large-scale shell model calculations exist [68] which show that the neutron polarization in ^{19}F is very close to zero (≈ -0.002) while the proton polarization is within $5 \pm 0.6\%$ of that of the whole nucleus. This is further corroborated by the magnetic moment, which is extremely close to that of a free proton. Targets could be made using ^{6}Li^{19}F. There is no reason not to expect that high polarization in ^{19}F can be achieved; however, the "dilution" due to the extra 24 other nucleons (only 2 of which may be slightly polarized) will make a precision experiment challenging. We are obviously not prepared to propose such an experiment at this time.

VI. BIBLIOGRAPHY

[1] Co-Spokesperson and Contact; email: william.brooks@usm.cl.
[2] Co-Spokesperson.
[3] J. J. Aubert *et al.*, Phys. Lett. B **123**, 275 (1983).
[4] S. Dasu *et al.*, Phys. Rev. D **49**, 5641 (1994).
[5] J. Gomez *et al.*, Phys. Rev. D **49**, 4348 (1994).
[6] U. Landgraf (NMC Collaboration.), Nucl.Phys. **A527**, 123C (1991).
[7] G. Bari *et al.* (BCDMS Collaboration), Phys.Lett. **B163**, 282 (1985).
[8] A. W. Thomas, A. Michels, A. W. Schreiber, and P. A. Guichon, Phys.Lett. **B233**, 43 (1989).
[9] F. Close, R. Jaffe, R. Roberts, and G. G. Ross, Phys.Rev. **D31**, 1004 (1985).
[10] C. Garcia Canal, E. Santangelo, and H. Vucetich, Phys.Rev.Lett. **53**, 1430 (1984).
[11] L. L. Frankfurt and M. I. Strikman, Phys. Rept. **160**, 235 (1988).
[12] O. Hen, D. Higinbotham, G. A. Miller, E. Piasetzky, and L. B. Weinstein, Int.J.Mod.Phys. **E22**, 1330017 (2013), arXiv:1304.2813 [nucl-th].
[13] I. Schmidt and J.-J. Yang, Eur.Phys.J. **C20**, 63 (2001), arXiv:hep-ph/0005054 [hep-ph].
[14] A. Daniel *et al.*, "Detailed studies of the nuclear dependence of F_2 in light nuclei," E12-10-008 approved by PAC 35.
[15] G. Petratos *et al.*, "Measurement of the F_{2n}/F_{2p}, d/u Ratios and $A = 3$ EMC Effect in Deep Inelastic Scattering off the Tritium and Helium Mirror Nuclei," E12-10-103 approved by PAC 36.
[16] J. Seely, A. Daniel, D. Gaskell, J. Arrington, N. Fomin, *et al.*, Phys.Rev.Lett. **103**, 202301 (2009), arXiv:0904.4448 [nucl-ex].
[17] A. V. Klimenko *et al.* (CLAS), Phys. Rev. C **73**, 035212 (2006), nucl-ex/0510032.
[18] O. Hen *et al.*, "In Medium Nucleon Structure Functions, SRC, and the EMC effect," E12-11-107 approved by PAC 38.
[19] D. F. Geesaman, K. Saito, and A. W. Thomas, Ann.Rev.Nucl.Part.Sci. **45**, 337 (1995).
[20] L. Frankfurt and M. Strikman, Int.J.Mod.Phys. **E21**, 1230002 (2012), arXiv:1203.5278 [hep-ph].
[21] R. Holt and R. Gilman, Rept.Prog.Phys. **75**, 086301 (2012), arXiv:1205.5827 [nucl-ex].
[22] M. Ericson and A. W. Thomas, Phys.Lett. **B128**, 112 (1983).
[23] C. Llewellyn Smith, Phys.Lett. **B128**, 107 (1983).
[24] D. de Florian, L. Epele, H. Fanchiotti, C. Garcia Canal, and R. Sassot, Z.Phys. **A350**, 55 (1994).
[25] I. Cloet, W. Bentz, and A. W. Thomas, Phys.Lett. **B642**, 210 (2006), arXiv:nucl-th/0605061 [nucl-th].
[26] W. Bentz, I. Cloet, T. Ito, A. Thomas, and K. Yazaki, Prog.Part.Nucl.Phys. **61**, 238 (2008), arXiv:0711.0392 [nucl-th].
[27] J. R. Smith and G. A. Miller, Phys.Rev. **C72**, 022203 (2005), arXiv:nucl-th/0505048 [nucl-th].
[28] V. Guzey and M. Strikman, Phys.Rev. **C61**, 014002 (2000), arXiv:hep-ph/9903508 [hep-ph].
[29] K. Ganesamurthy and R. Sambasivam, Nucl.Phys. **A856**, 112 (2011).
[30] H. Fanchiotti, C. Garca-Canal, T. Tarutina, and V. Vento, (2014), arXiv:1404.3047 [hep-ph].
[31] A. Airapetian *et al.* (HERMES Collaboration), Phys.Rev.Lett. **95**, 242001 (2005), arXiv:hep-ex/0506018 [hep-ex].
[32] K. Slifer *et al.*, "The Deuteron Tensor Structure Function b1," C12-13-011, conditionally approved by PAC 40.
[33] V. Dharmawardane *et al.*, "The EMC effect in spin structure functions," LOI-06-06 to PAC 29.
[34] W. Brooks *et al.*, "The EMC effect in Spin Structure Functions," LOI-10-005 to PAC 35.
[35] C. Ciofi degli Atti, L. Kaptari, and S. Scopetta, Eur.Phys.J. **A5**, 191 (1999), arXiv:hep-ph/9904486 [hep-ph].
[36] We are ignoring the third one, transversity h_1, which is not accessible in inclusive scattering.
[37] J. Soffer and O. Teryaev, (1999), arXiv:hep-ph/9906455 [hep-ph].
[38] X. Artru, M. Elchikh, J.-M. Richard, J. Soffer, and O. V. Teryaev, Phys.Rept. **470**, 1 (2009), * Temporary entry *, arXiv:0802.0164 [hep-ph].
[39] S. Wandzura and F. Wilczek, Phys.Lett. **B72**, 195 (1977).
[40] Landau, L.D. and Lifshitz, E.M., *Quantum Mechanics, Non-relativistic Theory* (Pergamon, New York, 1977).
[41] R. Wiringa, R. Schiavilla, S. C. Pieper, and J. Carlson, (2013), arXiv:1309.3794 [nucl-th].
[42] S. C. Pieper, R. B. Wiringa, and J. Carlson, Phys.Rev. **C70**, 054325 (2004), arXiv:nucl-th/0409012 [nucl-th].
[43] P. E. Bosted and M. E. Christy, Phys. Rev. C **77**, 065206 (2008).
[44] M. Christy and N. Kalantarians, (2013), in preparation.
[45] P. Jimenez-Delgado, A. Accardi, and W. Melnitchouk, Phys.Rev. **D89**, 034025 (2014), arXiv:1310.3734 [hep-ph].
[46] Y. Kahn, W. Melnitchouk, and S. A. Kulagin, Phys. Rev. C **79**, 035205 (2009).
[47] S. Tkachenko *et al.* (CLAS Collaboration), Phys. Rev. C **89**, 045206 (2014), arXiv:1402.2477 [nucl-ex].
[48] W. Cosyn, W. Melnitchouk, and M. Sargsian, Phys.Rev. **C89**, 014612 (2014), arXiv:1311.3550 [nucl-th].
[49] I. Cloet, W. Bentz, and A. W. Thomas, Phys.Rev.Lett. **95**, 052302 (2005), arXiv:nucl-th/0504019 [nucl-th].
[50] S. Kuhn, J.-P. Chen, and E. Leader, Prog.Part.Nucl.Phys. **63**, 1 (2009), arXiv:0812.3535 [hep-ph].
[51] S. Kuhn *et al.*, "The longitudinal spin structure of the nucleon," Experiment 12-06-109 at Jefferson Lab.
[52] V. Y. Alexakhin *et al.* (COMPASS Collaboration), Phys.Lett. **B647**, 8 (2007), arXiv:hep-ex/0609038 [hep-ex].
[53] J. Ball, G. Baum, P. Berglund, I. Daito, N. Doshita, *et al.*, Nucl.Instrum.Meth. **A498**, 101 (2003).
[54] K. Kondo, J. Ball, G. Baum, P. Berglund, N. Doshita, *et al.*, Nucl.Instrum.Meth. **A526**, 70 (2004).

[55] S. L. Bueltmann, D. Crabb, D. Day, R. Fatemi, B. Gardner, *et al.*, Nucl.Instrum.Meth. **A425**, 23 (1999).
[56] P. Anthony *et al.* (E155 Collaboration), Phys.Lett. **B463**, 339 (1999), arXiv:hep-ex/9904002 [hep-ex].
[57] M. Paolone, S. Malace, S. Strauch, I. Albayrak, J. Arrington, *et al.*, Phys.Rev.Lett. **105**, 072001 (2010), arXiv:1002.2188 [nucl-ex].
[58] S. Jeschonnek and J. W. Van Orden, Phys. Rev. C **78**, 014007 (2008).
[59] W. P. Ford and J. W. Van Orden, Phys. Rev. C **87**, 014004 (2013).
[60] M. Mayer, *Beam-Target Double Spin Asymmetry in* $\vec{d}(\vec{e}, e'p)n$, Ph.D. thesis, Old Dominion University (2013).
[61] D. Crabb and W. Meyer, Ann.Rev.Nucl.Part.Sci. **47**, 67 (1997).
[62] M. Moteabbed *et al.* (CLAS Collaboration), Phys.Rev. **C88**, 025210 (2013), arXiv:1306.2286 [nucl-ex].
[63] J. Lachniet *et al.* (CLAS Collaboration), Phys.Rev.Lett. **102**, 192001 (2009), arXiv:0811.1716 [nucl-ex].
[64] Y. Prok *et al.* (CLAS Collaboration), (2014), arXiv:1404.6231 [nucl-ex].
[65] L. W. Mo and Y. S. Tsai, Rev. Mod. Phys. **41**, 205 (1969).
[66] T. Kukhto and N. Shumeiko, Nucl.Phys. **B219**, 412 (1983).
[67] I. Akushevich and N. Shumeiko, J.Phys.G **G20**, 513 (1994).
[68] P. Klos, J. Menndez, D. Gazit, and A. Schwenk, Phys.Rev. **D88**, 083516 (2013), arXiv:1304.7684 [nucl-th].